AD-A053 571 STANFORD UNIV CALIF DEPT OF MATERIALS SCIENCE AND EN--ETC F/G 11/6
FINE STRUCTURE AND SUPERPLASTICITY IN ULTRAHIGH CARBON STEELS.(U)
DEC 77 J WADSWORTH, J T LO, B WALSER N00014-77-C-0149

UNCLASSIFIED NL

1 OF 1
ADA
053571

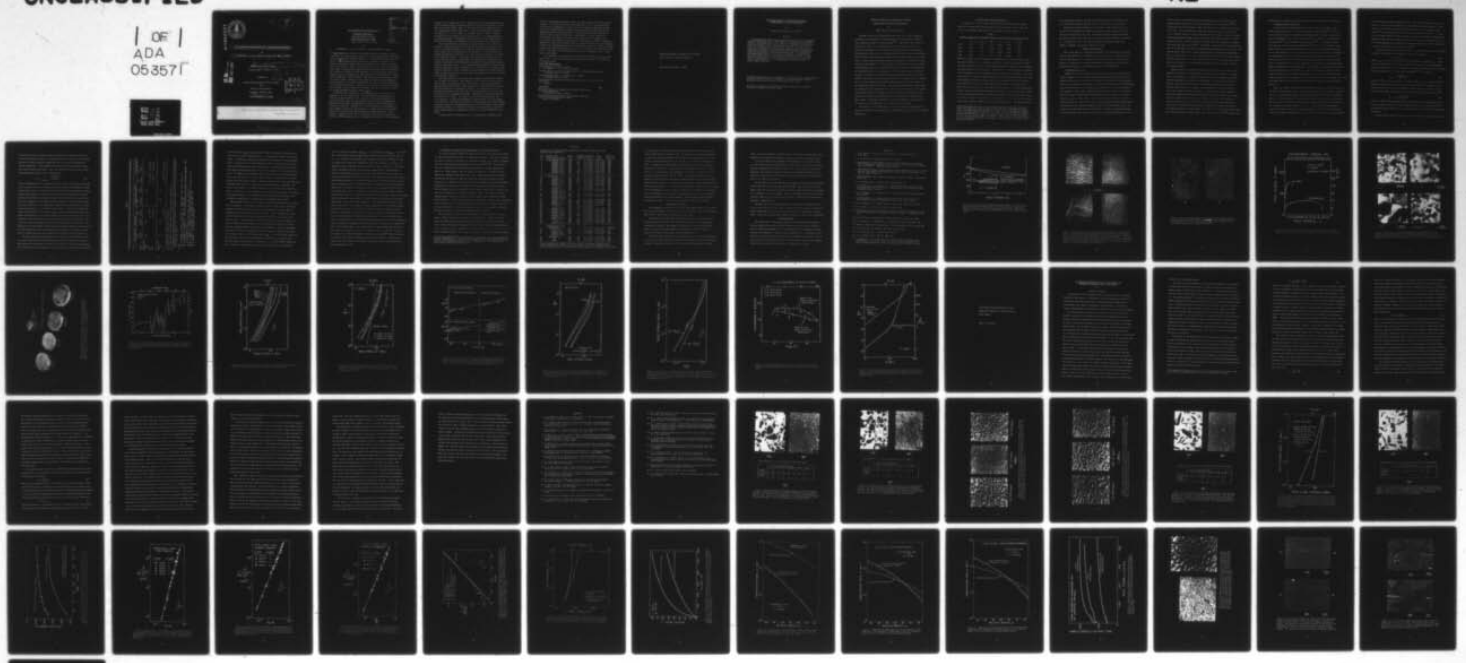

END
DATE
FILMED
6-78
DDC

FINE STRUCTURE AND SUPERPLASTICITY IN ULTRAHIGH CARBON STEELS

By

J. WADSWORTH, J.T. LO, B. WALSER, R. CALIGIURI AND O.D. SHERBY

First Annual Progress Report, no. 1, 1 Jan-31 Dec 77,

January 1, 1977 - December 31, 1977

31 Dec 77

submitted to

69 p.

Defense Advanced Research Projects Agency

and

Office of Naval Research

Arlington, Virginia, 22217

(Contract N00014-77-C-0149)

Department of MATERIALS SCIENCE AND ENGINEERING
STANFORD UNIVERSITY

FINE STRUCTURE AND SUPERPLASTICITY IN ULTRAHIGH CARBON STEELS

(Contract N00014-77-C-0149)

FIRST ANNUAL PROGRESS REPORT

(Jan. 1, 1977 - Dec. 31, 1977)

By

J. Wadsworth, J. T. Lo, B. Walser, R. Caligiuri and O. D. Sherby

This program has centered on the thermal-mechanical processing of steels containing 1 to 2.3%C and their properties. These ultrahigh carbon (UHC) steels have been commercially neglected because of a traditional belief that they are brittle. The processing however leads to the formation of extremely fine cementite particles of about 1/10 micron (0.0001 mm) in a matrix of extremely fine ferrite grains of about 1 micron (0.001 mm) or less. This fine structure lends itself to several unique and exciting characteristics which revolutionize the traditional attitudes to these materials. In the first place these fine grained steels are superplastic at warm temperatures and elongations to failure of over 1500% have now been obtained. This means that these materials can be very easily formed. Second, they are strong and ductile at room temperature and the strength can be simply controlled by the final processing temperature or subsequent heat treatment. Third, they can be given a simple transformation heat treatment to form a structure of cementite and martensite which is about as hard ($R_c \cong 65$-68) as tungsten carbide.

During the first half year of our program we have concentrated on the chemistry of our UHC carbon steels. Specifically we have investigated the influence of small additions of Cr, V, Mn, Si, and Ni on the properties of fine grained UHC steels. We have discovered that Ni and Si are undesireable additions for they enhance graphitization leading to inferior warm and low temperature properties. Addition of Cr, V and Mn appears to be desirable for these elements stabilize the carbides that are formed and fine ferrite grains remain fine even after long time deformation at warm temperatures. These changes in composition have lead to considerable improvement in superplastic behavior (~1000% elongation) and in room temperature ductility (~20% elongation)

compared to our original UHC steels. The mode of failure at warm temperatures is also improved; whereas a finite reduction of area was noted earlier, the new UHC steels usually exhibit 100% R.A. Our new results are summarized in the first semi-annual progress report (Jan. 1, 1977 to June 30, 1977) authored by J. Wadsworth, J. T. Lo, B. Walser, R. Caligiuri and O. D. Sherby. Further optimization of the chemistry of our steels as well as the thermal-mechanical processing treatment for enhancement of superplastic and room temperature properties will represent an important part of our studies in our second year.

This report describes two aspects of our work in UHC steels. The first portion is a paper which describes the mechanical behavior of superplastic UHC steels at elevated temperature. The paper was prepared by Bruno Walser and Oleg D. Sherby and is being submitted for publication. In the manuscript the strength and ductility characteristics of UHC steels are assessed in the temperature range 600 to 850°C. It was shown that the flow stress-strain rate relations obtained at various temperatures were quantitatively described by the additive contributions of grain boundary (superplastic) creep and slip (lattice diffusion controlled) creep. It was predicted that superplastic characteristics should be observed at normal forming rates for the UHC steels if the grain size could be stabilized at 0.4μm. The UHC steels were found to be readily rolled or forged at high strain rates in the warm range of temperatures even in the as-cast, coarse grained, condition.

The second portion of this annual report summarizes the doctoral dissertation of Robert D. Caligiuri. This subject is on the pressure sintering kinetics of iron powders and superplastic UHC steel powders. Caligiuri convincingly demonstrates that densification under pressure sintering conditions is enhanced when the powders have a superplastic structure. His studies have lead to a generalized relation for the prediction of the densification rate if the creep characteristics of the powders are known. Specifically, the densification rate is given by $\dot{\rho} \simeq 60 \left(\frac{1-\rho}{\rho}\right)^n \cdot \dot{\varepsilon}_{ss}$ where $\dot{\rho}$ is the relative densification rate, ρ is the density, n is the stress exponent for creep flow and $\dot{\varepsilon}_{ss}$ is the steady state creep rate. Caligiuri's work leads to the possibility of pressure bonding superplastic materials at temperatures where solid state bonding is not normally considered possible. He illustrates the perfect bond attainable in UHC steels after pressure bonding at temperatures below the A_1 critical temperature (e.g. 650°C).

A further aspect of Caligiuri's work is the superplastic bonding of UHC

steels to other ferrous materials. There are unique features to such solid state joining. In the first place the bonding temperature is very low, always below the critical A_1 temperature (~723°C). This is an important temperature because below it no phase changes occur and hence desirable starting structures are not significantly affected during bonding. The bonding itself is also greatly enhanced by the fact that the UHC steel is superplastic. In the second place, if UHC steels are bonded to low carbon steels (mild steel for example) then the product can be selectively heat treated. For instance, by taking a laminated composite of a UHC steel and mild steel to a temperature above the A_1 and quenching, a product of transformed UHC steel and unaffected mild steel will result (it should be noted that some interdiffusion will occur at the interface at temperatures above 723°C). This aspect of our study on UHC steels will be emphasized in the second year of our program.

The following is an outline of the four sections that made up the first semi-annual report. This is then followed by the two sections that are described in this annual report:

FIRST SEMI-ANNUAL REPORT

Superplasticity in 52100 tool steel,
J. Wadsworth, J. T. Lo, and O. D. Sherby

Influence of Ni, Cr, and V, on Superplasticity in Ultrahigh Carbon Steels
J. Wadsworth and O. D. Sherby

Ultrahigh Carbon Steels - The Influence of Chromium
J. Wadsworth and O. D. Sherby

Experimental work performed on Ultrahigh Carbon Steels at Sulzer Brothers, Switzerland
B. Walser

THIS REPORT

Mechanical Behavior of Superplastic Ultrahigh Carbon Steels at Elevated Temperature

Bruno Walser and Oleg D. Sherby

MECHANICAL BEHAVIOR OF SUPERPLASTIC ULTRAHIGH CARBON STEELS AT ELEVATED TEMPERATURE

by

Bruno Walser* and Oleg D. Sherby**

Abstract

Ultrahigh carbon (UHC) steels were investigated for their strength and ductility characteristics from 600 to 850°C. It was shown that such UHC steels, in the carbon range 1.3 to 1.9%C, were superplastic when the microstructure consisted of fine equiaxed ferrite or austenite grains (~1μm) stabilized by fine spheroidized cementite particles. The flow stress-strain rate relations obtained at various temperatures were quantitatively described by the additive contributions of grain boundary (superplastic) creep and slip (lattice diffusion controlled) creep. It was predicted that superplastic characteristics should be observed at normal forming rates for the UHC steels if the grain size could be stabilized at 0.4μm. The UHC steels were found to be readily rolled or forged at high strain rates in the warm and hot range of temperatures even in the as-cast, coarse grained, condition.

* Formerly Research Associate, Department of Materials Science and Engineering, Stanford University, Stanford, California, now Research Manager, Physical Metallurgy Group, Sulzer Brothers, Wintherthur, Switzerland.

** Professor, Department of Materials Science and Engineering, Stanford University, Stanford, California, 94305.

Mechanical Behavior of Superplastic Ultrahigh Carbon Steels at Elevated Temperatures

by

Bruno Walser and Oleg D. Sherby

Recently a new class of ultrahigh carbon steels (1.3-1.9%C), combining superplastic characteristics at elevated temperature with good to excellent room temperature properties, was developed[1-4]. The basis of our success in making plain carbon steels superplastic was the attainment of ultra fine structures with grain sizes in the order of 0.5 to 5μm in size and cementite particles about 0.1μm in size. The high volume fraction of cementite particles present (20 to 35 volume percent) maintains the fine grain size at warm temperature. Several thermal-mechanical processing methods were developed to obtain these fine structures[1,2]. Not only should such hypereutectoid steels exhibit superplasticity below the A_1 critical temperature, 723°C, but they should also be superplastic above the A_1 temperature. This desirable result is possible because the austenite grains obtained upon transformation should also be fine grained (since many nuclei exist from the prior fine grained ferrite). Furthermore, the fine austenite grains should remain fine because of the presence of the undissolved cementite particles. This condition should yield a wide range of temperature where superplastic flow can be expected and Figure 1 illustrates the possible influence of carbon on the expected range for superplastic flow. Thus, for a 1.9%C steel, superplasticity may be expected to be observed from 600 to 850°C, a desirable characteristic from the viewpoint of flexibility in the manipulation of temperature for superplastic metal forming.

The purpose of the present paper is to present, describe and assess the mechanical properties of ultrahigh carbon (UHC) steels (1.3 to 2.3%C) at elevated temperatures.

Materials and Experimental Procedure

Castings of 1.3, 1.6, 1.9 and 2.3%C steels* were obtained in the form of slabs 33.5 cm long wherein the dimensions of the bases were 5 by 5 cm and 5 by 2.5 cm. The chemical composition of the castings are given in Table I.

Table I

Chemical Composition of Ultrahigh Carbon Steels Investigated (weight percent)

	C	Mn	Si	P	S	Fe
1.3%C	1.25	0.65	0.10	0.016	0.024	bal.
1.6%C	1.57	0.73	0.28	0.015	0.020	bal.
1.9%C	1.92	0.82	0.30	0.018	0.019	bal.
2.3%C	2.28	0.80	0.31	0.017	0.020	bal.

Examples of carbon replica transmission photographs of the as-cast microstructure are shown in Figure 2 for a 1.6% and a 1.9%C steel. One observes massive primary cementite networks; oftentimes, a well developed pearlite structure is seen adjoining the proeutectoid cementite particles. The influence of extensive mechanical working on the refinement of the cast microstructure is shown in the same figure. The 1.6%C steel exhibits a uniformly spheroidized structure. This sample was heated to 1150°C and deformed continuously at 10% per pass to a true strain of 2.0 as it cooled to about 600-650°C; it was then isothermally rolled at 650°C, 5% per pass, to an additional true strain of 1.5. The worked 1.9%C steel was not as fully spheroidized as the 1.6%C steel (lower right photograph in Figure 2). This was, in part, attributed to insufficient working in the alpha range (only 0.9 true strain in this case). An example of optical micrographs for a 1.9%C steel in the as-cast state and after extensive alpha working at 650°C ($\varepsilon = 1.5$) is shown in Figure 3. The grain size for a

* The 2.3%C composition steel is more correctly defined as cast iron since most definitions place cast irons as alloys of iron and carbon containing more than 1.7%C. The significance of this level of carbon is that it formerly was thought to be the maximum solubility of carbon in γ iron. In the early 1940's, however, the maximum solubility of carbon in γ iron was shown to lie at about 2% and the current, widely accepted, value is 2.11%C[5]. Since we make only minimal reference to the 2.3%C composition alloy in this paper we will classify it as part of the UHC steels studied.

fully spheroidized steel in the UHC steels investigated is in the order of 0.5 to 1.5μm and the cementite particle sizes are in the order of 0.1 to 0.5μm.

Rectangular tensile specimens were used, with a gage section of 12.7 or 25.4 mm length and different thicknesses depending on the thickness of the as-rolled plate (typically 2 to 5 mm). Transmission electron microscope studies were done by spark cutting thin plates from tested samples followed by grinding to a thickness of 0.1 mm. The final electrolytic thinning was done in an Na_2CrO_4 - CH_4COOH - electrolyte at 20°C and 25 volts.

Results and Discussion

Most of the mechanical tests were performed in the temperature range from 600°C to about 850°C where superplastic effects were noted. In this section we will discuss the nature of the stress-strain curves observed, the flow stress-strain rate relations noted below and above the A_1 temperature and lastly, the influence of strain rate and temperature on the tensile ductility.

1) Stress-strain curves

Examples of true stress-true strain curves obtained for the 1.6%C steel are shown in Figure 4. In this figure the fully spheroidized fine grained steel is compared with the as-cast material. The samples were deformed at an engineering strain rate of 1% per minute at 650°C. We note the high ductility (500% elongation) and low flow stress of the fine grained steel compared to the coarse grained as-cast material. These results follow the expected behavior, that is, fine superplastic structures exhibit lower strengths than coarse structures at elevated temperature and low strain rates. Two results were noted, however, which were somewhat unexpected. The first relates to the considerable strain hardening that was observed to occur during superplastic flow of the fine grained steels. For example, the flow stress more than doubled (30 to 65 MPa) after 200% elongation. We attribute this result to grain growth that occurred during superplastic flow

since it is well established that coarse grained samples are stronger than fine grained samples (typically σ is directly proportional to the grain size[6-8]). Transmission electron microscopy studies revealed that the original grain size was about 0.5μm. After deformation to 100% elongation, the grain size increased to 1.5 to 2 microns and after a total elongation of 300% the grain size was about 3μm. These microstructural changes during superplastic straining were typical of those noted for the 1.3, 1.6 and 1.9%C steels although other, less sensitive, variables were strain rate and temperature[4]. An example of grain growth during superplastic flow of a 1.9%C steel is shown in the transmission photomicrographs of Figure 5. Of special note in this figure is that straining enhances grain growth dramatically. Thus, the grip region of the tested sample (Figure 5D), where no straining occurred, exhibits a grain size of 1μm after exposure to the same time at temperature; this grain size is about three times smaller than that observed in the gage region of the fractured sample.

Another interesting observation in Figure 4 is that the as-cast 1.6%C steel exhibited a respectably high elongation to fracture of 43% at 650°C ($T = 0.51T_m$). Such a result suggests that UHC steel castings are rather forgiving materials at elevated temperature and should not crack easily. This agreed well with our experience since edge cracking rarely occurred during rolling in the temperature range of 550°C to 1100°C. An example of the forgeability of the UHC steels in the as-cast condition is shown in Figure 6. Castings in the form of machined cubes were forged at 850°C in one step (about 3 to 5 seconds forging time) to the capacity of the press used, 170 tons force (1.52 MN). None of the samples exhibited cracking except the 2.3%C steel. The latter steel, which contains 34 volume percent cementite below the A_1 point, could not be worked extensively at any temperature without cracking badly. It is not at all clear why such difficulties were observed with this carbon content steel, although recent work[9] suggests that

diminishing the presence of silicon may contribute to inhibition of edge cracking.

2) Change-in-strain rate tests

A common method of determining the flow stress-strain rate relation from a single superplastic sample is to perform strain-rate change tests[10]. This is a very convenient method and is especially meaningful when structural changes do not occur during plastic flow. This is often not the case, however, as emphasized by Rai and Grant[11] and by Baudelet and his colleagues[12]. We mentioned earlier that grain growth occurred during superplastic deformation of the ultrahigh carbon steels (Figure 5) and that this was responsible for the strain hardening observed in the early portion of the true stress-true strain curve (Figure 4). We developed an experimental method which helped to minimize this problem by predeforming the material to a strain of 0.2 to 0.4 at which point a steady state flow-stress (and hence a steady state structure) was approached. The sample was then deformed small amounts at several different strain rates. In this manner a large amount of information was obtained between the flow stress and the corresponding strain rate over a range of strain where grain growth was minimal. The flow stress observed at each strain rate was assumed to represent a given constant grain size. An example of a strain rate change test for the 1.6%C steel in the gamma plus cementite range is shown in Figure 7.

Strain rate change tests performed at different temperatures for the 1.6%C steel are presented in Figure 8 as flow stress-strain rate curves. The influence of carbon content on the flow stress-strain rate relationship for the UHC steels is shown in Figure 9. These data reveal the normal trend expected in superplastic materials at low strain rates, namely the stress exponents are low and typical of those observed for superplastic metallic alloys (i.e. $n \simeq 2$). In this region, grain boundary sliding is believed to be the rate controlling process in plastic flow and elongations in the order of 500-700% were noted. At high strain rates, the stress exponents

were typically about eight (Figures 8 and 9). Note the wide range of strain rates where $n \simeq 8$ for the coarse grained ($d = 10\mu m$) iron-carbon alloy (Figure 9). These values can be compared with stress exponents noted in constant structure creep tests[14] at high temperature; one can assume that constant structure is maintained in the UHC steel since the submicron grain size present would make it unlikely that subgrains would form and at high strain rates virtually no grain growth occurs. In this region deformation by slip processes involving dislocation climb is believed to be the rate determining step for plastic flow[14].

The above results suggest that the creep rate of the UHC steels can be correlated by means of two additive contributions to plastic flow, namely:

$$\dot{\varepsilon} = \dot{\varepsilon}_{sp.f.} + \dot{\varepsilon}_{s.c.} \tag{1}$$

where $\dot{\varepsilon}_{sp.f.}$ is the creep rate associated with superplastic flow and $\dot{\varepsilon}_{s.c.}$ is the creep rate associated with slip creep. Specific expressions have been developed to describe these relations. The superplastic flow rate of fine grain size materials, when grain boundary diffusion is rate-controlling[6,7,15], is given by

$$\dot{\varepsilon}_{sp.f.} = A \frac{b D_{gb}}{d^3} \left(\frac{\sigma}{E}\right)^2 \tag{2}$$

where $A \simeq 10^8$, d is the grain size, b is Burgers vector, D_{gb} is the grain boundary diffusion coefficient in the matrix phase of the superplastic material, σ is the creep stress and E is the unrelaxed dynamic Young's modulus. The creep rate in the slip creep range, where lattice diffusion is rate controlling is given by[13]

$$\dot{\varepsilon}_{s.c.} = A' \left(\frac{\lambda}{b}\right)^3 \frac{D_L}{b^2} \left(\frac{\sigma}{E}\right)^8 \tag{3}$$

where $A' \simeq 10^9$ for high stacking fault energy materials, λ is the subgrain size or barrier spacing (in the case of the ultrahigh carbon steel the grain size or the interparticle spacing whichever is the finest), and D_L is the lattice self-diffusion coefficient.

The data shown in Figure 8 were plotted to determine the activation energy for

plastic flow in the two regions in order to compare the results with those predicted by equations (2) and (3). The method selected to calculate the activation energy was to plot the modulus compensated flow stress versus the reciprocal absolute temperature. This permitted using data within the superplastic region and within the slip creep region. Thus, the activation energy for plastic flow, from equations (2) and (3), can be calculated by

$$Q\Big|_{\dot{\varepsilon} = \text{constant}} = \frac{R \, d\ln \left(\frac{\sigma}{E}\right)^n}{d \, 1/T} \tag{4}$$

Plots for determination of the activation energy are given in Figures 10A and 10B. As can be seen, the activation energy for plastic flow in the superplastic region (Figure 10B) is about 160 kjoules per mole in both the alpha plus cementite region and gamma plus cementite region; these values are nearly identical to the grain boundary self diffusion activation energy of iron in alpha iron, 170 kjoules per mole, and in gamma iron, 163 kjoules per mole (Table II). The activation energy for plastic flow in the slip creep region (Figure 10A) was determined to be about 350 kjoules per mole from the limited data available. This value is higher than those noted by Kayali[13] for creep of coarse grained ultrahigh carbon steel where values of 250 kjoules per mole were obtained. This discrepancy may be due to the possibility that slip creep is not yet the dominating deformation process at the strain rate used to determine the activation energies given in Figure 10A. These differences not withstanding, we associate the activation energy for plastic flow in the slip creep region with the activation energy for lattice diffusion in alpha iron, 251 kjoules per mole, and in gamma iron, 270 kjoules per mole (Table II).

The above calculations yield qualitative evidence that the UHC steels behave in a manner predicted by the phenomenological creep flow relations (2) and (3). More importantly, a quantitative prediction can be made. Thus, the creep behavior of the 1.6%C steel in the alpha plus cementite region can be predicted by equations

TABLE II

Grain Boundary, Lattice Diffusion and Modulus Data for Iron in the Ferrite and Austenite Phase Regions

	Grain Boundary Diffusion[1]			Lattice Diffusion[2]			Elastic Modulus
T(°C)	D_o cm^2/sec	Q kj/mole	D_{gb} cm^2/sec	D_o cm^2/sec	Q kj/mole	D_L cm^2/sec	E (G) MPa
Alpha iron + Fe_3C	17.7	170		1.6	252		
650			4.1×10^{-9}			9.0×10^{-15}	1.61×10^5
700			1.3×10^{-8}			5×10^{-14}	1.52×10^5
Gamma iron + Fe_3C	1.8	163		0.18	270		
770			1.2×10^{-8}			4×10^{-14} (3)	1.35×10^5

(1) Average values, based on Ref. A, B and C.

(2) Average values taken from a number of sources quoted in reference (D)

(3) Extrapolation of pure gamma iron data (T>910°C) down to 770°C, then multiply by seven because of the enhancement of gamma iron self diffusion by carbon in solution at 770°C (0.8 w/o C) as determined from reference E and F

(4) Ref.

(A) C. Leymonie, Y. Adda, A. Kirianenko, P. LaCombe, Compt. Rend. 248, (1959) 1512.
(B) D. W. James, G. H. Leak, Phil. Mag., 12, (1965) 491.
(C) P. LaCombe, P. Guiraldeng, C. Leymonie, Radioisotopes in the Physical Science Industry, (1962) I.A.E.A. Vienna, 179.
(D) O. D. Sherby, P. M. Burke, Progr. Mater. Sci., 13, (1967) 333.
(E) P. L. Gruzin, R. V. Kornev, G. V. Kurdimov, Dokl. Acad. Nauk., USSR, 80 (1957) 49.
(F) H. W. Mead, C. E. Birchenall, Trans. AIME, 206 (1956) 1336.
(G) W. Koster, Z. fur Metallkde, 39, (1948) 1.

(2) and (3) since D_{gb} and D_L are known for alpha iron (Table II) and since the grain size, d, and the barrier spacing, λ, are known after plastic flow in this region. As mentioned previously, grain growth occurred due to the superimposed effect of strain and time in the superplastic region; grain sizes in the superplastically deformed samples were typically 2μm. In the high strain rate slip creep region, grain growth did not occur and the grain size was typically 0.5 to 1.0μm. To compare the experimental flow stress-strain rate data with equations (2) and (3), the grain size, d, was chosen as 2μm to substitute into the superplastic flow rate expression and λ = 0.5μm was chosen for the slip creep flow rate expression (the interparticle spacing was taken as the barrier spacing). The result of the prediction is shown in Figure 11 for the 1.6%C steel at 650°C and 700°C. As can be seen, good quantitative correlations were obtained, attesting to the probable validity of the superplastic flow and slip creep relations in describing the creep behavior of fine grain size ultrahigh carbon steels.

The strength difference of the 1.6%C steel above and below the A_1 is readily seen in Figure 10. Extrapolation of the data in this figure to the transition temperature reveals that the UHC steel in the gamma plus cementite region is stronger than in the alpha plus cementite region. This is probably due to the lower diffusion rate in the face-centered-cubic austenitic steel than in the ferritic steel. It was decided to compare the stress-strain rate relation for the UHC steel both above and below the A_1 by selecting a temperature at which the grain boundary diffusion coefficients were identical. The two temperatures selected were 700°C for the alpha plus cementite range and 770°C for the gamma plus cementite range. At these temperatures, $D_{gb} \simeq 1.2 \times 10^{-8}$ cm^2/sec (Table II). By coincidence, the lattice self diffusion coefficients in the ferritic and austenitic phases were also nearly identical, $D_L \simeq 5 \times 10^{-14}$ cm^2/sec (Table II). And, the dynamic Young's modulus values for pure iron in the two crystalline

forms are also quite similar, $(E_\gamma)_{770°C} = 1.35 \times 10^5$ MPa and $(E_\alpha)_{700°C} = 1.52 \times 10^5$ MPa. (The modulus value for gamma iron at 770°C should be corrected for the 0.9 wt % C in solution at this temperature; no modulus data appear available to make the appropriate calculation, although the correction is likely to be small.) A comparison of the 1.6%C steel at 700 and 770°C is shown in Figure 12. The curves nearly superimpose attesting to the previous suggestion that the appropriate diffusion coefficients (D_{gb} and D_L) and the elastic moduli properly account for the plastic flow behavior of the 1.6%C steel. The lower creep rate of the austenitic phase material compared to the ferritic phase material in the superplastic region can be attributed to a grain size difference; it is possible that grain growth is enhanced in the austenite region because there is less cementite present than in the ferrite region (12.5 vol % Fe_3C at 770°C compared to 25 vol % Fe_3C at 700°C). At high strain rates in the slip creep region, the ferritic phase material is stronger than the austenitic phase material. Several factors can contribute to the latter observation. First, the barrier spacing (i.e. the interparticle spacing and the grain size) in the ferrite range is probably smaller than in the austenite range; (if equation (3) is used to predict the difference in barrier spacing from the difference in strength, about a factor of two is calculated.) We believe this to be the most likely factor influencing the difference in strength at high strain rates. A second factor is that solid solution hardening (e.g. atom size differences) from the presence of manganese and silicon may be more effective in the austenitic than in the ferritic phase. And, a third factor is the possible contribution of the hardness of cementite per se to the strength of the iron-cementite composite that makes up the 1.6%C steel studied. That is, it is known[16] that the hardness of cementite is an order of magnitude higher than the hardness of alpha iron at 700°C but is only a factor ot two harder than gamma iron when the hardness data are extrapolated to 770°C.

3) Influence of strain rate and temperature on the tensile ductility

The above discussion reveals that UHC steels when in fine grained form exhibit all the characteristics expected of a superplastic material. The tensile ductility increased in value as the strain rate sensitivity exponent, m, increased, following the usual trends described extensively in the literature[17,18]. We give the results of isostrain-rate tests performed to determine the tensile elongation in Table III. These tabulated data are plotted in Figure 13 as tensile ductility against the diffusion compensated strain rate. Elongations as high as 750% were obtained for the UHC steels when the strain rate sensitivity exponents reached values of 0.5. Samples tested in the ferrite plus cementite range exhibited higher elongations, as an average, than samples in the austenite plus cementite range. This difference is likely attributable to the slightly coarser grain size that may exist in the austenite range than in the ferrite range. All samples exhibited necking prior to failure; the fracture region, however, never exhibited a chisel point failure (i.e. reduction of area was less than 100%). This was rather surprising since no evidence of cracking was observed in the UHC steels in regions away from the fractured region. Regions adjoining the fracture surface, however, exhibited presence of minute voids mostly at interphase boundary sites*.

The UHC steels studied in this investigation are superplastic up to strain rates as high as 10% per minute (Table III and Figure 13). Although these are respectably high strain rates, they are not in the order of commercial forming rates. From a practical and economical point of view it would be highly desirable if the UHC steels could be superplastic at normal forming rates, i.e. 10^{-1} to 1 sec^{-1} (600 to 6000% per minute). Such a goal is a realistic one and the principal method

* Recent investigations[19] have revealed that appropriate control of chemical composition (primarily low silicon content and small additions of carbide stabilizing elements like vanadium) can lead to tensile elongations exceeding 1500% and to chisel point type fractures (100% R.A.).

Table III

Elongations to fracture for the superplastic ultrahigh carbon steels under different test conditions.*

Test No.	Material and alpha working history	Test T (°C)	Initial Strain-rate $\dot{\varepsilon}$(%min^{-1})	$\dot{\varepsilon}$ (Sec^{-1})	$\dot{\varepsilon}/D_{gb}$, cm^{-2}	elon. to frac. (%)
1	1.3%C αw(650) εα=1.7	605	1	1.7×10^{-4}	2.2×10^{6}	230
2	αw(650) εα=1.2	630	0.8	1.3×10^{-4}	4.85×10^{4}	700
3	αw(650) εα=1.2	650	0.8	1.3×10^{-4}	3.17×10^{4}	600
4	αw(650) εα=1.2	650	1	1.7×10^{-4}	4.15×10^{4}	480
5	αw(650) εα=1.2	650	1	1.7×10^{-4}	4.15×10^{4}	250
6	αw(565) εα=1.7	650	10	1.7×10^{-3}	4.15×10^{5}	320
7	αw(565) εα=0.8	650	100	1.7×10^{-2}	4.15×10^{6}	76
8	αw(565) εα=1.7	800	10	1.7×10^{-3}	7.94×10^{4}	140
9	1.6%C αw(565) εα=1.5	600	10	1.7×10^{-3}	1.38×10^{6}	207
10	αw(650) εα=1.7	620	0.4	6.7×10^{-5}	3.22×10^{4}	489
11	αw(650) εα=1.7	630	0.8	1.3×10^{-4}	4.85×10^{4}	760
12	αw(650) εα=1.7	650	0.4	6.7×10^{-5}	1.63×10^{4}	473
13	αw(650) εα=1.7	650	1	1.7×10^{-4}	4.15×10^{4}	486
14	αw(565) εα=1.0	650	1	1.7×10^{-4}	4.15×10^{4}	334
	as cast	650	1	1.7×10^{-4}		43
16	αw(650) εα=1.7	650	4	6.7×10^{-4}	1.63×10^{5}	532
17	αw(650) εα=1.7	650	10	1.7×10^{-3}	4.15×10^{5}	457
	αw(500) +100 Hrs					
18	/500°C εα=1.7	650	10	1.7×10^{-3}	4.15×10^{5}	273
19	αw(565) εα=1.0	650	10	1.7×10^{-3}	4.15×10^{5}	270
	αw(700) +100 Hrs					
20	/500°C εα=1.3	650	10	1.7×10^{-3}	4.15×10^{5}	240
21	αw(650) εα=1.1	650	100	1.7×10^{-2}	4.15×10^{6}	78
22	αw(650) εα=1.7	670	0.4	6.7×10^{-5}	9.6×10^{3}	361
23	αw(650) εα=1.1	700	10	1.7×10^{-3}	1.3×10^{5}	262
24	no αw	700	10	1.7×10^{-3}		73
25	αw(565) εα=1.0	750	200	3.3×10^{-2}	3.75×10^{6}	83
26	αw(650) εα=1.7	770	1	1.7×10^{-4}	1.41×10^{4}	421
27	αw(650) εα=1.8	770	1	1.7×10^{-4}	1.41×10^{4}	165
28	αw(650) εα=1.8	770	10	1.7×10^{-3}	1.41×10^{5}	183
29	αw(650) εα=1.8	770	100	1.7×10^{-2}	1.41×10^{6}	89
30	αw(565) εα=1.5	800	1	1.7×10^{-4}	7.93×10^{3}	234
31	αw(565) εα=1.5	800	10	1.7×10^{-3}	7.93×10^{4}	397
32	no αw	800	10	1.7×10^{-3}	7.93×10^{4}	120
33	αw(565) εα=1.5	800	100	1.7×10^{-2}	7.93×10^{5}	165
	1.9%C αw(650) εα=0.9					
34	+700°C/30 min	650	1	1.7×10^{-4}	4.15×10^{4}	378/380
35	αw(565) εα=0.2	650	1	1.7×10^{-4}	4.15×10^{4}	231
36	αw(565) εα=1	650	1	1.7×10^{-4}	4.15×10^{4}	334
37	αw(593) εα=1.1	650	1	1.7×10^{-4}	4.15×10^{4}	328
	αw(650) εα=0.9					
38	+700°C/30 min	700	10	1.7×10^{-3}	1.3×10^{5}	222
39	same	650	10	1.7×10^{-3}	4.15×10^{5}	254
40	same	770	10	1.7×10^{-3}	1.41×10^{5}	195

* all ultrahigh carbon steels were first worked by continuous rolling from an initial temperature of 1200°C to a final temperature of 650°C achieving a total true strain of about two. The subsequent working treatment is described in the table.

of achieving it is to develop a grain size finer than one micron in size which remains stable during superplastic flow. We illustrate our concept graphically in Figure 14, utilizing equations (2) and (3) to make the predictions. In this figure we show the strain rate-stress relation for our 1.6%C steel deformed at 700°C. As mentioned previously the average grain size of this steel during superplastic flow is 2μm. If the grain size is decreased by a factor of five, that is, to a size of 0.4μm, the superplastic flow rate, at a given stress, is enhanced by over a hundred fold ($5^3 = 125$). The resulting strain rate-stress relation for the 0.4μm grain size steel, shown in Figure 14, is such that superplastic flow now extends to a strain rate of about 1 per second. Clearly this is a desirable end objective. We are currently attempting to stabilize the fine grain size by appropriate control of chemical composition. The effort is centering on the role of manganese and silicon in retarding cementite particle agglomeration (which then leads to ferrite grain growth). Alloying elements which stabilize the carbide in steels, such as V, Ti, Cr and Nb are also being considered.

Summary and Conclusions

The superplastic properties of ultrahigh carbon (UHC) steels (1.3 to 1.9%C) have been investigated in the ferrite as well as austenite range of temperatures, 600 to 800°C. The following characteristics were noted:

(1) The UHC steels exhibited strain hardening during superplastic flow at all temperatures of testing. This was attributed to grain coarsening during superplastic straining. For example, the ferrite grain size increased from 0.5μm to about 2.0μm during superplastic deformation at 650°C, although it remained remarkably stable without concurrent deformation.

(2) At low strain rates, the stress exponent, n, in $\dot{\varepsilon} \propto \sigma^n$, was observed to be about two, a value generally attributed to superplastic flow by grain boundary sliding. At high strain rates, the stress exponent was observed to be about

eight, a value we attribute to plastic flow by a slip creep mechanism where grain boundaries and cementite particles are considered as barriers to plastic flow.

(3) In the range where superplastic flow dominates, the activation energy was found equal to about 170 kjoules/mole a value nearly equal to that for grain boundary self-diffusion in alpha or gamma iron. In the range where slip creep dominates, the activation energy was found to be considerably higher than 170 kjoules per mole and was identified with the activation energy for lattice self-diffusion in alpha or gamma iron.

(4) The tensile ductility was high at low values of the diffusion-compensated strain rate, with elongations equal to 300 to 750%. The tensile ductility was higher below the A_1 temperature (ferrite-cementite range) than above the A_1 temperature (austenite - cementite range). This was attributed to the lower content of cementite above the A_1 than below the A_1 leading to enhanced grain growth in the austenite - cementite range.

The UHC steels exhibited high ductility at warm and hot temperatures even in the as-cast coarse structure state. No edge cracking was noted in large strain forging experiments on the as-cast carbon steels even at temperatures as low as 850°C. These results suggest that such UHC steels have a wide range of workability.

Acknowledgements

The authors wish to acknowledge support of the Defense Advanced Research Projects Agency and the Office of Naval Research in this program of research. They are especially grateful to Drs. E. Van Reuth and B. A. MacDonald for their guidance and cooperation. Thanks are also extended to Dr. J. Wadsworth for his assistance in various phases of the work on the ultrahigh carbon steels. One of the authors (B.W.) would like to thank the Swiss Federal Institute of Technology (ETH-Zurich), especially to Professor Dr. W. Epprecht, for support.

References

1. O. D. Sherby, B. Walser, C. M. Young and E. M. Cady, Scripta Met., 9, 1975, 569.

2. U. S. Patent No. 3,951,697 issued April 20, 1976.

3. Bruno Walser, E. Sabri Kayali and Oleg D. Sherby, Conference Proceedings, Fourth International Conference on the Strength of Metals and Alloys, Nancy, France, 30 August - 3 September 1976, 456-460.

4. Bruno Walser and Oleg D. Sherby, Second Annual Technical Report, July 1, 1974-June 30, 1975, Defense Advanced Research Projects Agency, Washington, D. C., Grant No. DAHC-14-73-G15.

5. Metals Handbook, Eighth Edition, 8, American Society for Metals, Metals Park, Ohio, 275.

6. C. M. Packer and O. D. Sherby, Trans. ASM, 60, 1967, 21.

7. J. E. Bird, A. K. Mukherjee and J. E. Dorn, Quantitative Relation between Properties and Microstructure, D. G. Brandon and A. Rosen, editors, Israel University Press, 1969, 255.

8. J. W. Edington, K. N. Melton and C. P. Cutler, Progress in Materials Science, 21, 1976, 61.

9. J. Wadsworth and O. D. Sherby, research in progress, to be reported at Western Metals Congress, Los Angeles, Calif., March 20-23, 1978.

10. W. A. Backofen, J. R. Turner and D. H. Avery, Trans. ASM, 57, 1964, 980.

11. G. Rai and N. J. Grant, Met. Trans., 6A, 1975, 385.

12. B. Baudelet, Conference Proceedings, Fourth International Conference on the Strength of Metals and Alloys, Nancy, France, 30 August - 3 September 1976, 1, 2.

13. S. Kayali, Ph.D. dissertation, Stanford University, Calif., July 1976.

14. O. D. Sherby, R. H. Klundt and A. K. Miller, Met. Trans., 8A, 1977, 843.

15. Richard A. White, Ph.D. dissertation, Stanford University, Calif. March 1978.

16. K. G. Gove and J. A. Charles, Met. Tech., 1, 1974, 229.

17. D. A. Woodford, Trans. ASM, 62, 1969, 291-293.

18. W. B. Morrison, Trans. ASM, 61, 1968, 423.

19. J. Wadsworth, J. T. Lo, B. Walser, R. Caligiuri and O. D. Sherby, First Annual Report, Jan. 1, 1977 - Dec. 31, 1977, Defense Advanced Research Projects Agency and Office of Naval Research, Contract N00014-77-C-0149.

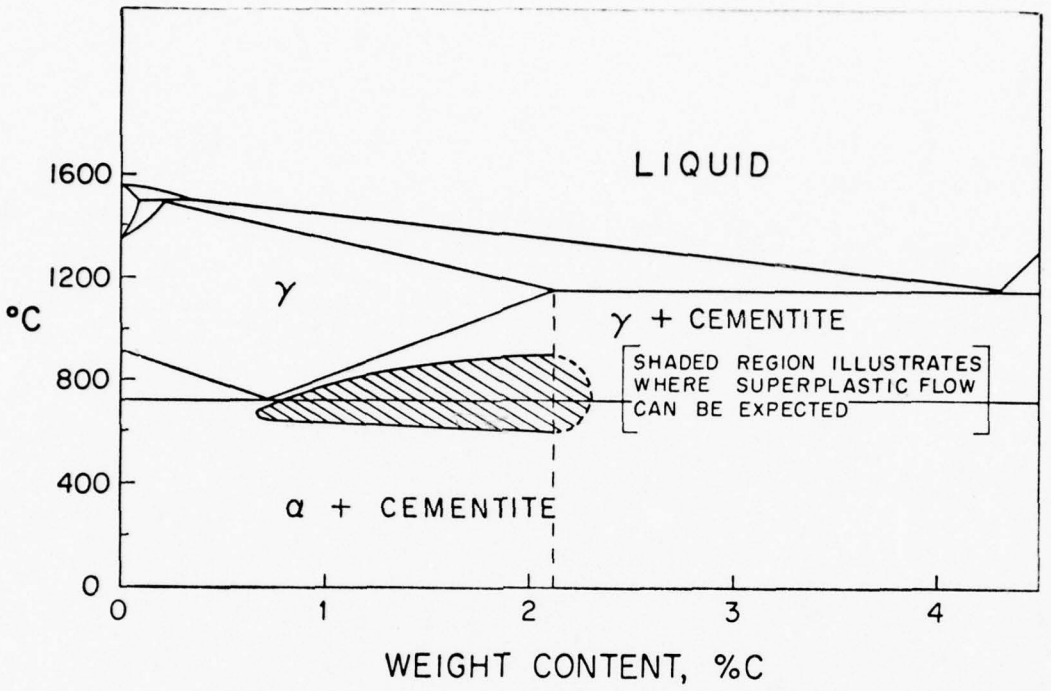

Figure 1. Iron-carbon phase diagram illustrating range of carbon contents and temperature where superplastic flow can be expected. Fine grained hypereutectoid steels, stabilized by the presence of fine particles of cementite, can be expected to be superplastic over a wide range of temperatures.

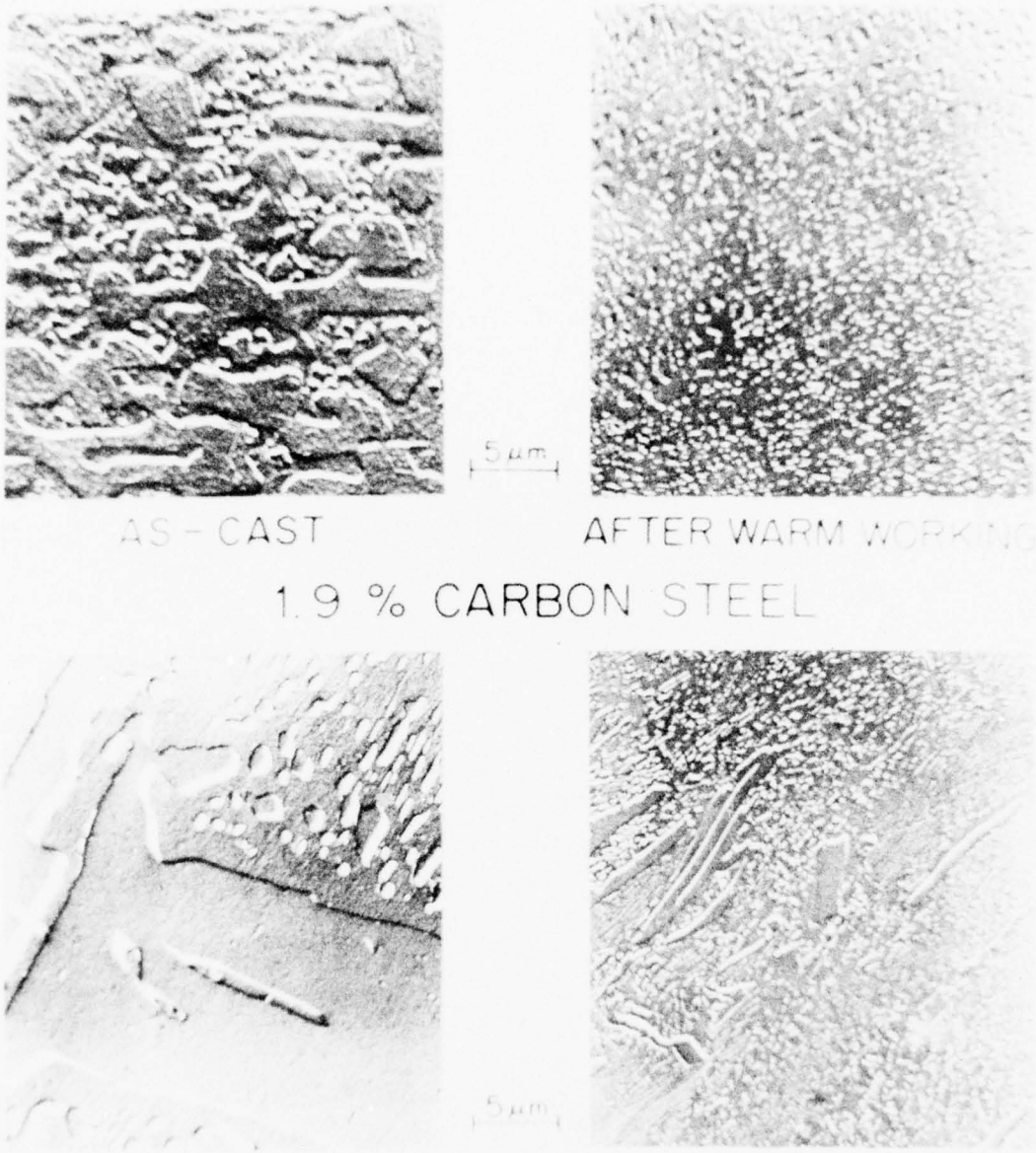

Figure 2. The above carbon replica electron photomicrographs illustrate the influence of warm working on the breakup of the original massive cementite particles in cast ultrahigh carbon steels (left photomicrographs). Extensive warm working yielded a fully spheroidized structure in the 1.6% carbon steel (upper right). Considerable refinement of the structure occurred in the 1.9% carbon steel (lower right) by warm working but because it was not extensively worked some cementite plates are still present.

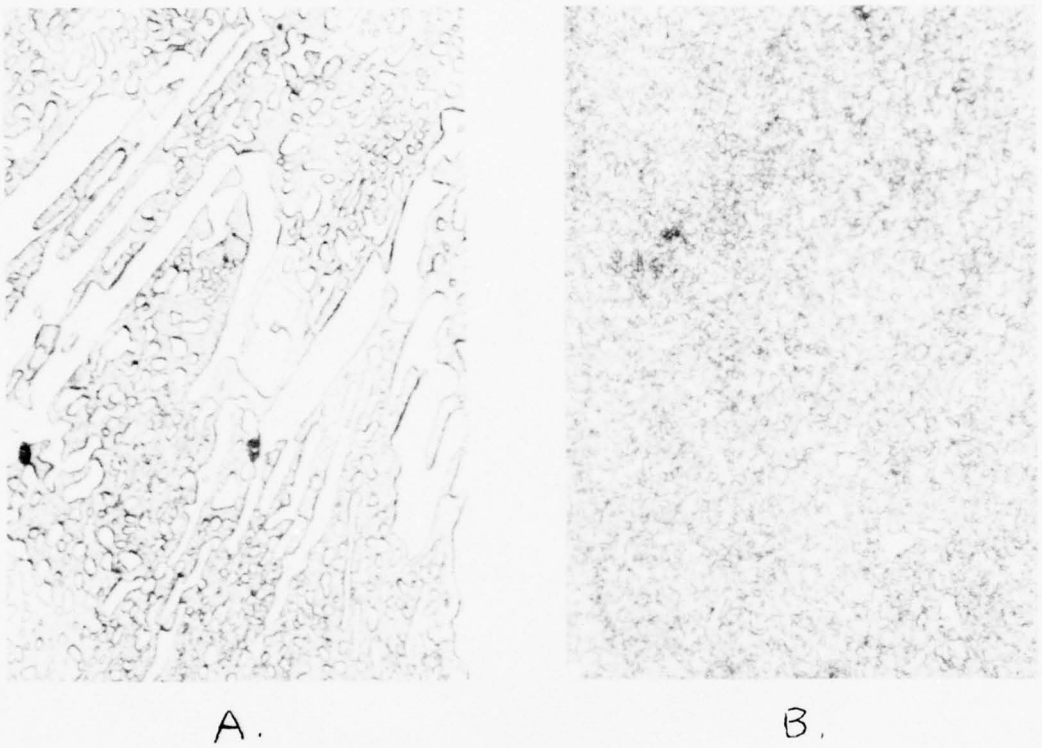

Figure 3. Optical photomicrographs of 1.9%C steel, illustrating change in microstructure from coarse proeutectoid [redacted] cementite structure in as-cast condition (A) to equiaxed fine grained state in extensively hot and warm worked condition (B). Magnification 1550X.

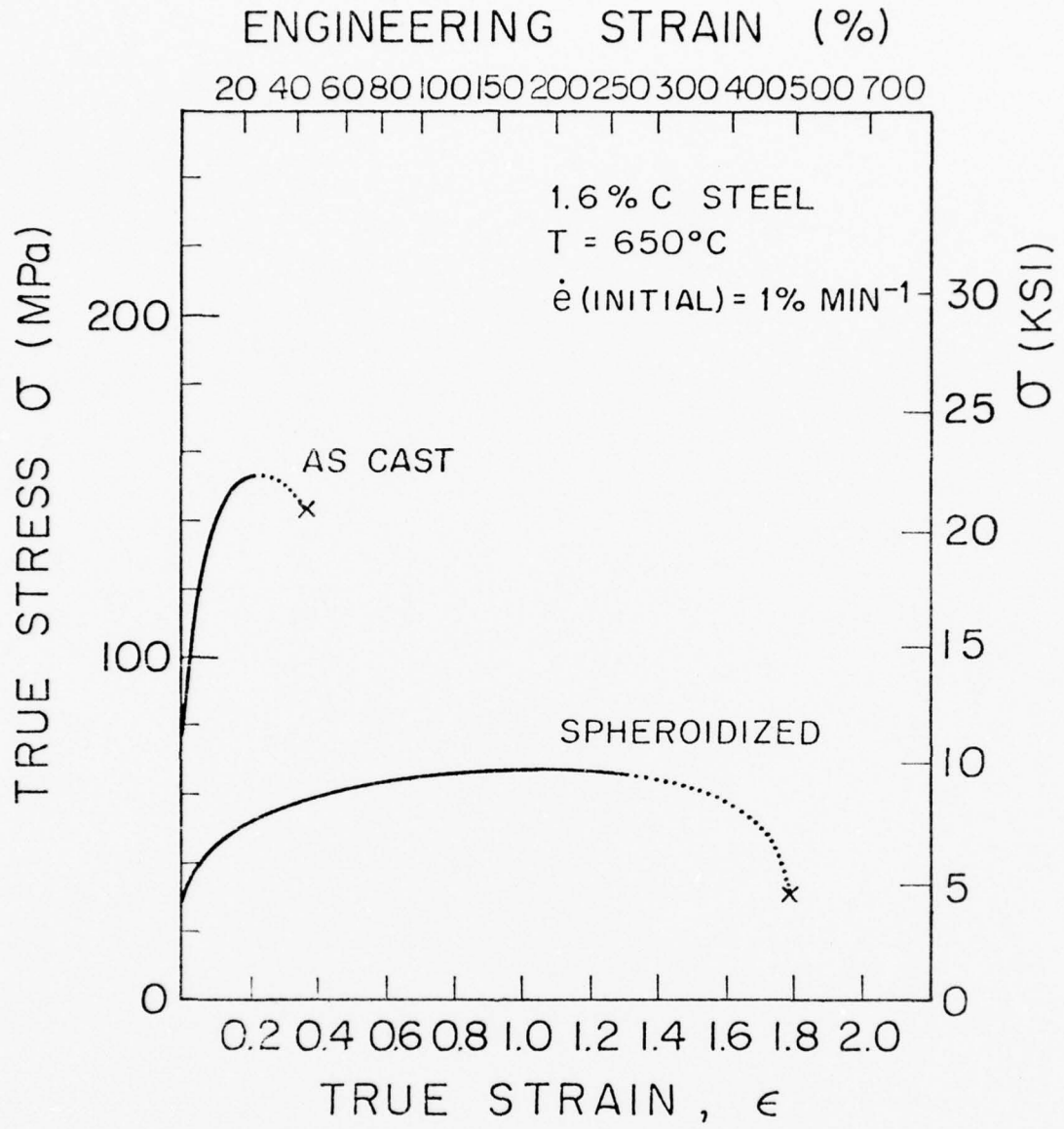

Figure 4. True stress-true strain curves at 650°C for a 1.6%C steel in coarse grained as-cast state and in spheroidized fine-grained conditions.

0.5 μm

A - as rolled

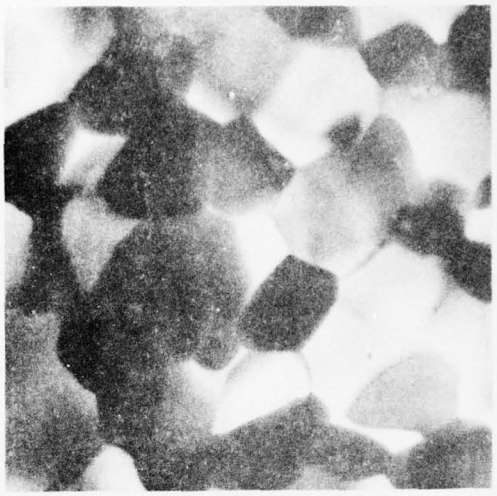

B - e = 100%

1 μm

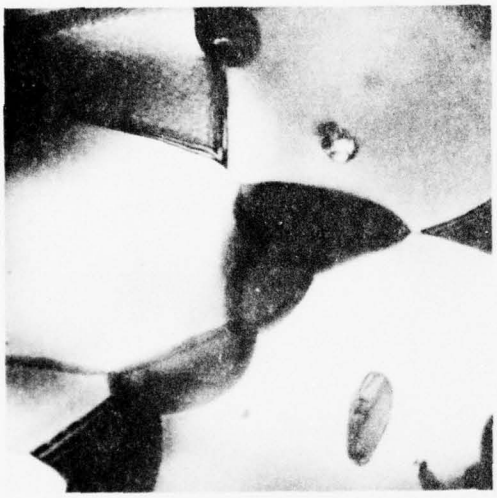

C - e = 200%

1 μm

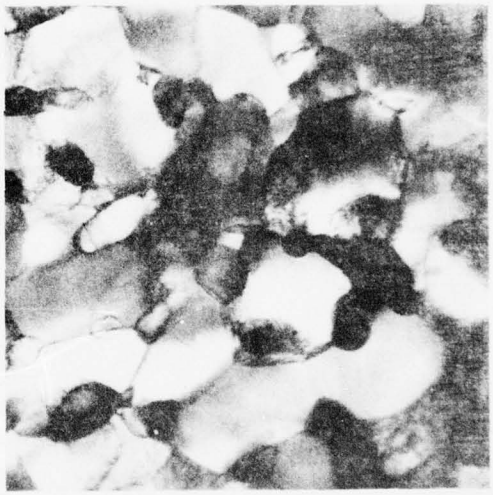

D - grip region of sample C.

1 μm

Figure 5. Transmission electron micrographs of a warm worked 1.9%C steel illustrating the grain growth that occurs during superplastic flow. (A) steel in as-rolled condition $(\gamma w)_C + \alpha w$ at 650°C), (B) and (C) superplastically deformed at 650°C and $\dot{e}$ = 1% per minute, (D) grip region of sample shown in (C).

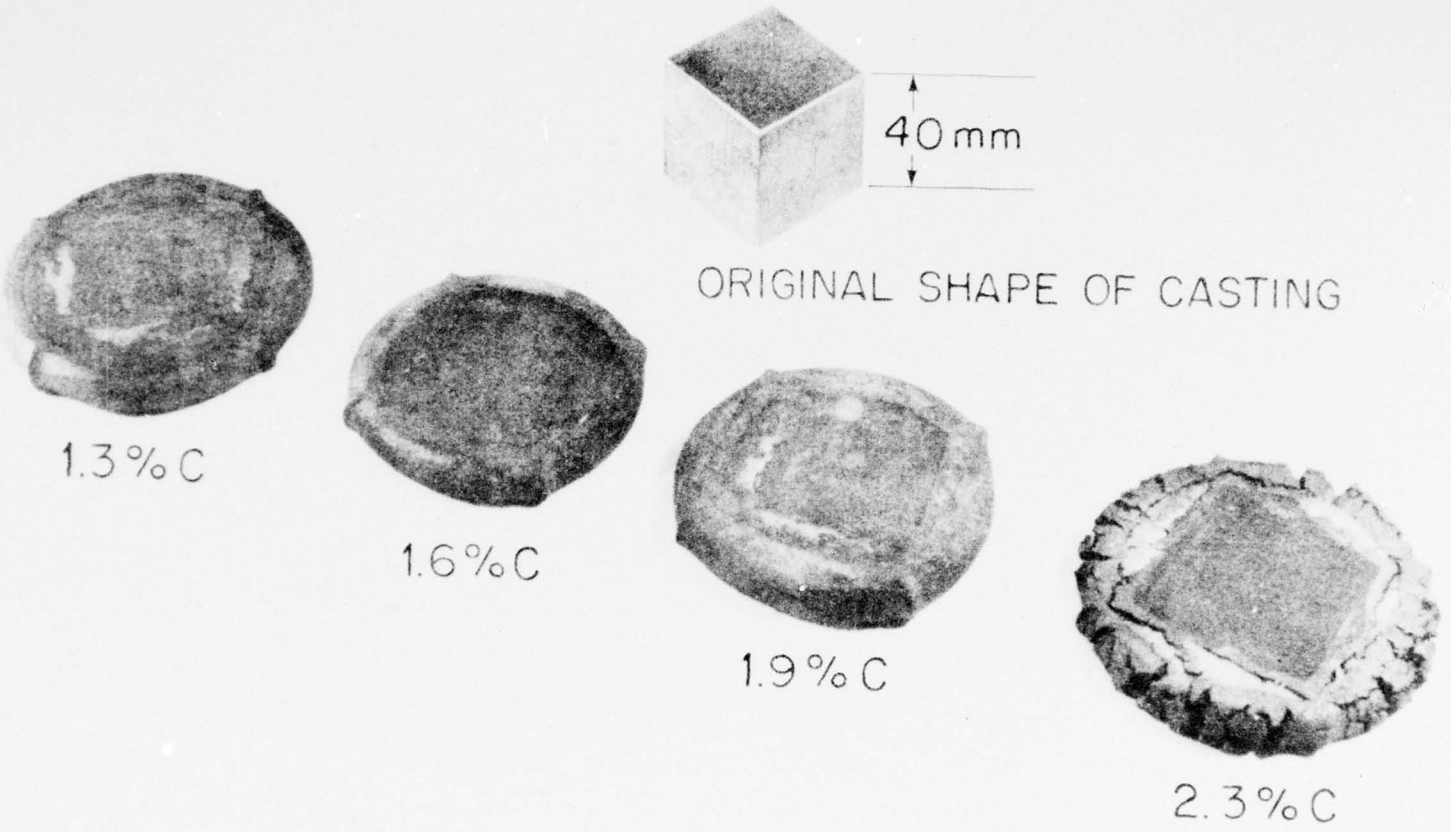

Figure 6. The UHC steels investigated exhibit great ease of formability even in the as-cast state. The above illustrates the lack of edge cracking after one rapid forging step, to a strain of about 1.2, at 850°C. Only the 2.3%C steel exhibited edge cracking.

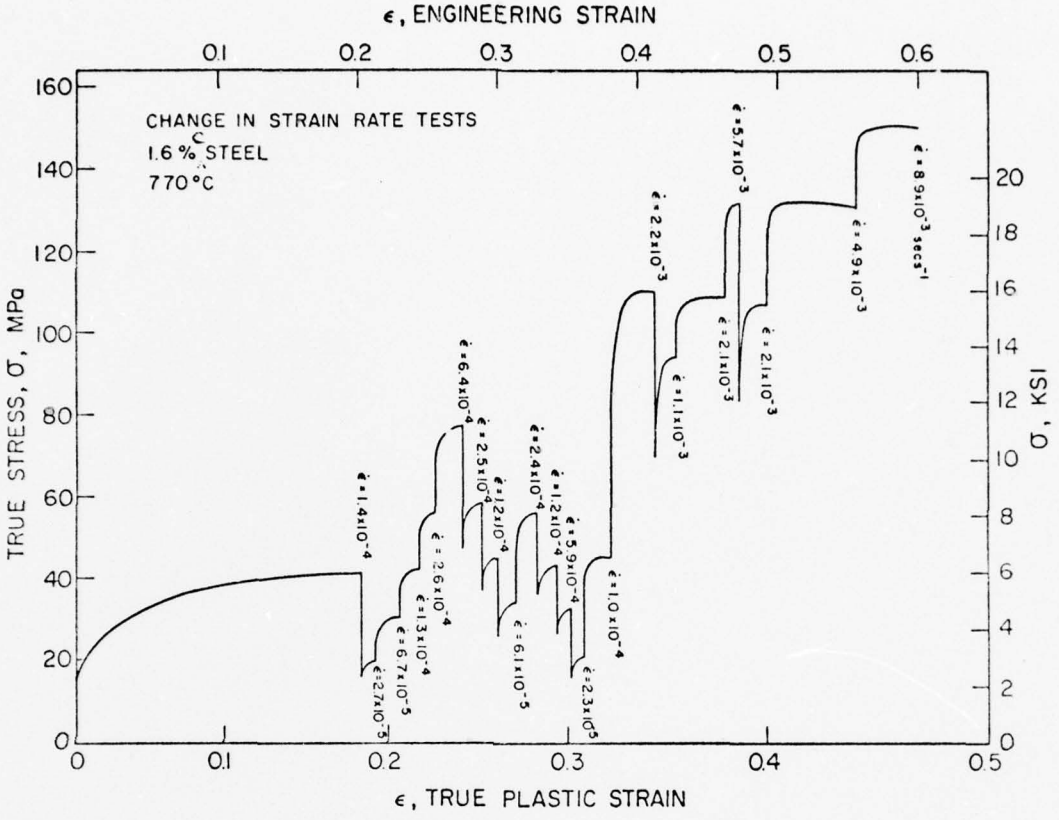

Figure 7. The above illustrates change-in-strain-rate tests performed to determine the flow stress-strain rate relation at constant structure. The example shown is for a 1.6%C steel tested in the austenite-cementite range (770°C).

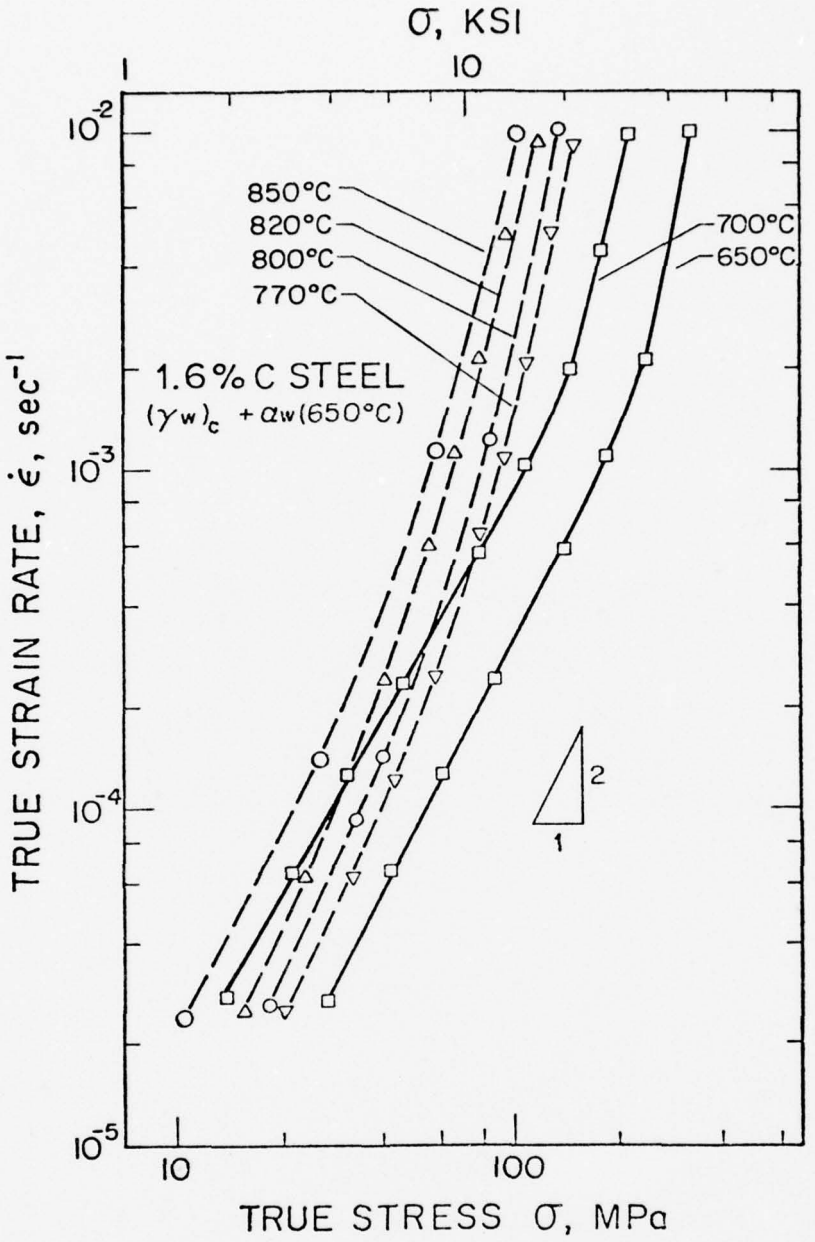

Figure 8. Flow stress-strain rate relation for fine grained 1.6%C steel in the ferrite-cementite and austenite-cementite temperature range.

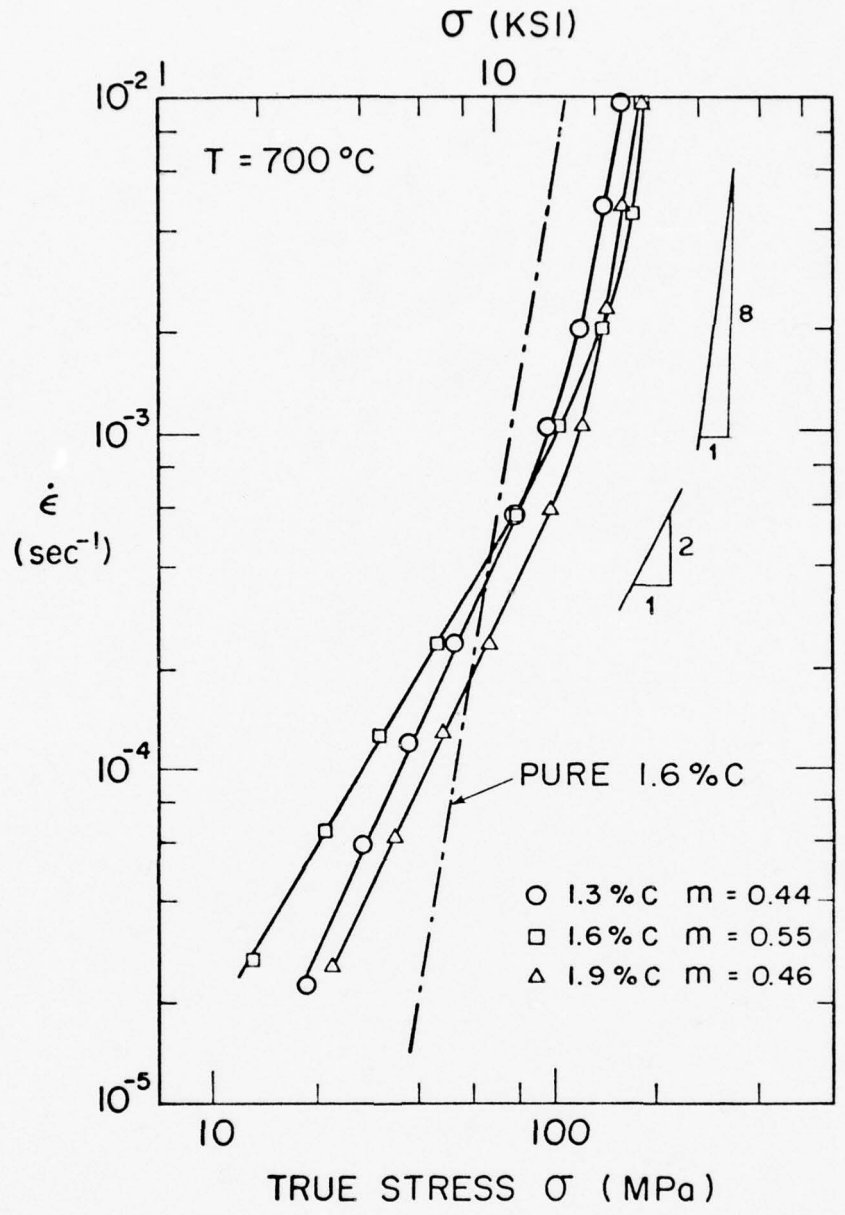

Figure 9. Influence of carbon content on the flow stress-strain rate relationship for fine-grained UHC steels at 700°C. Note the wide range of strain rate where n ≈ 8 for the coarse grained (d ≈ 10μm) iron-carbon alloy[13].

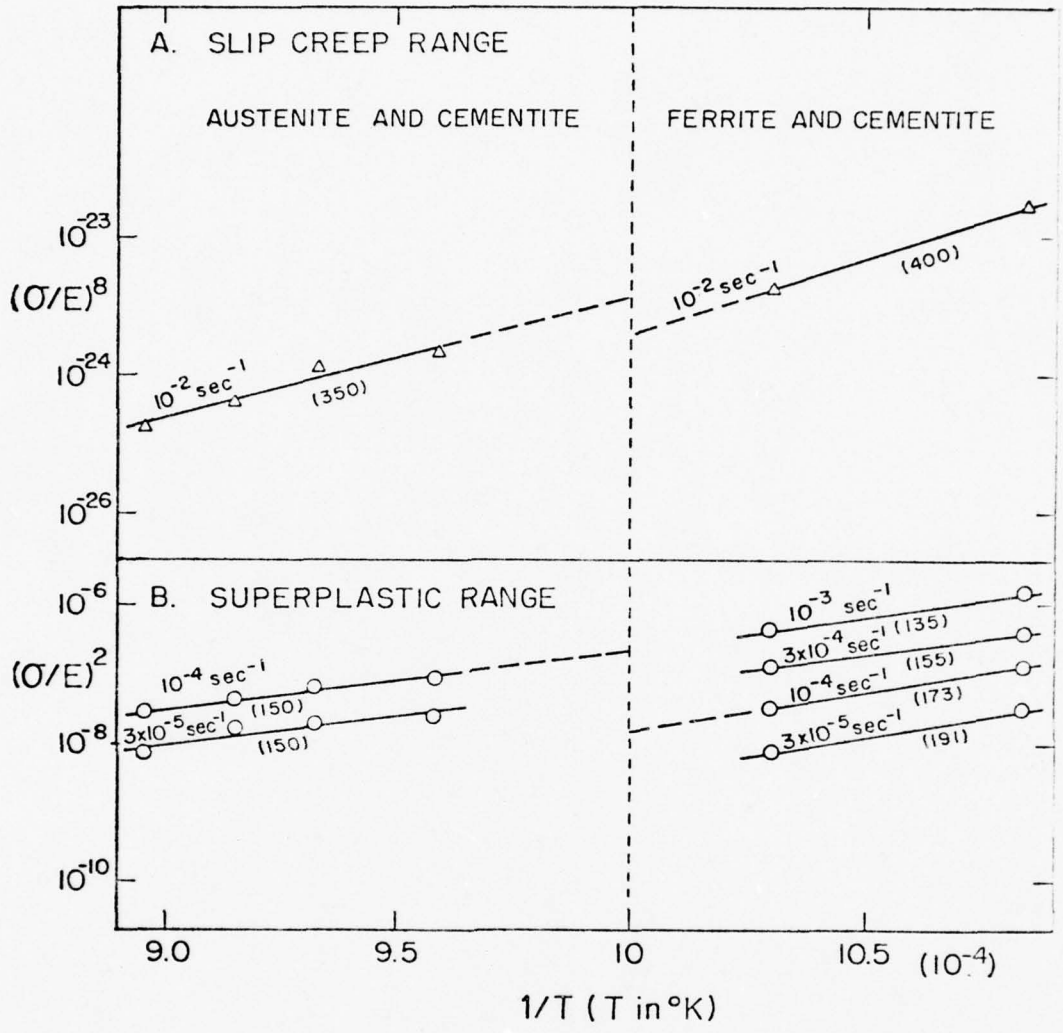

Figure 10. Activation energy for plastic flow calculated from plots of modulus compensated stress as a function of reciprocal absolute temperature. Values of activation energy are given in parenthesis (kjoules per mole) in the slip creep range and in the superplastic range.

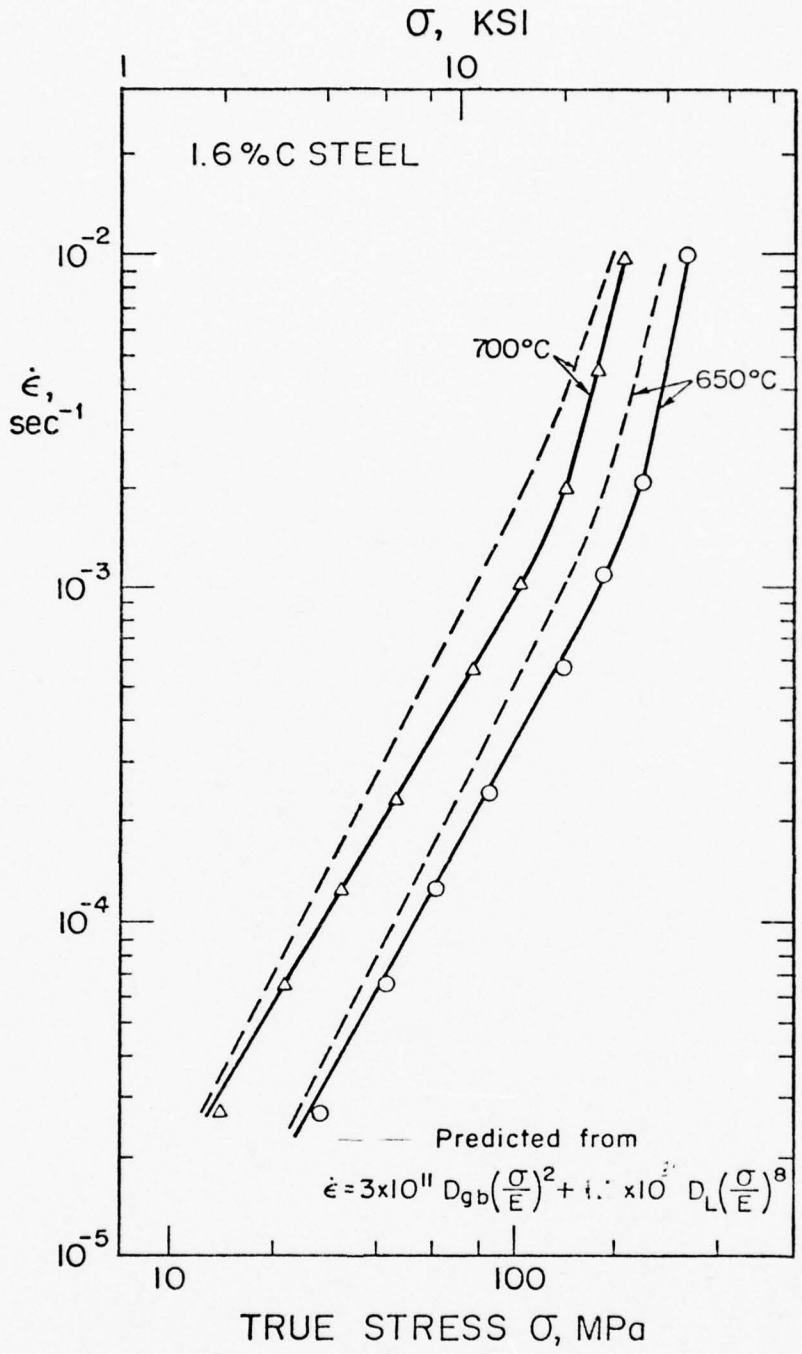

Figure 11. The flow stress-strain rate relationship for fine grained 1.6%C steel is compared with that predicted from the additive contribution of slip creep and superplastic creep [equations (2) and (3)]. Burgers vector was assumed equal to 2.5Å.

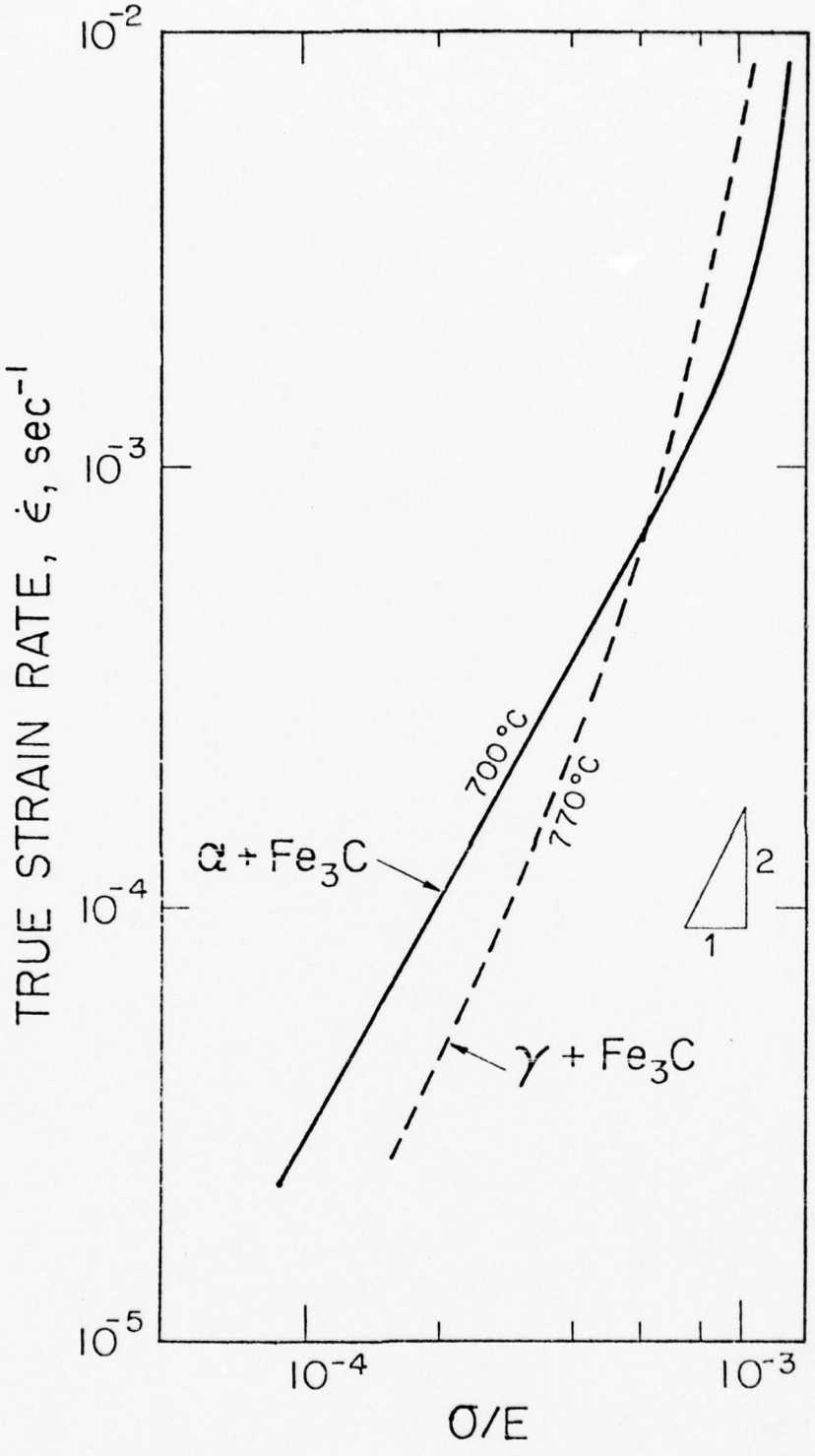

Figure 12. The modulus compensated flow stress-strain rate relationship for 1.6%C steel is compared at 770°C (austenite-cementite range) and at 700°C (ferrite-cementite range) where the diffusion coefficients are nearly identical. The small difference in the resulting curves can be primarily attributed to a difference in grain size.

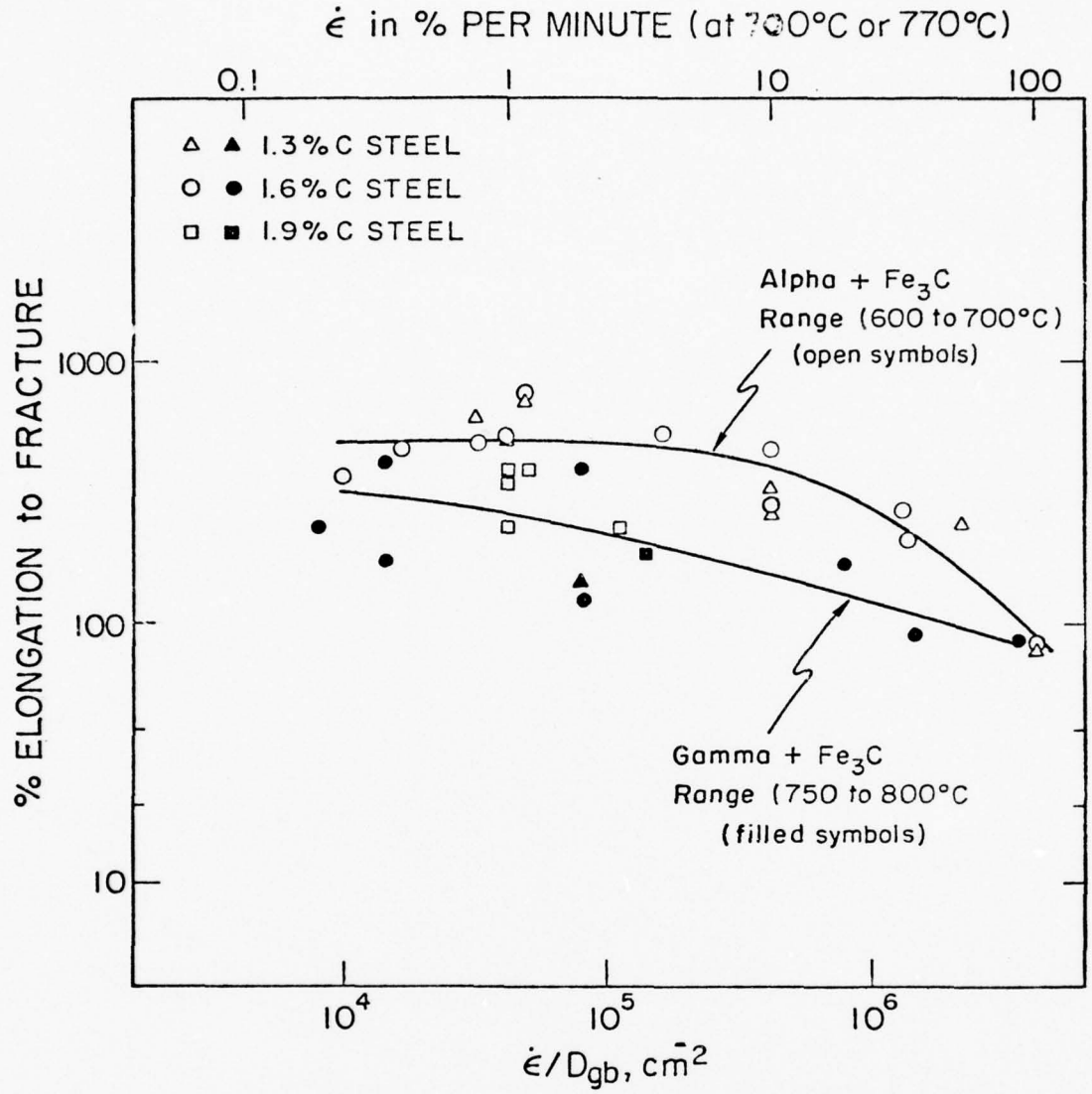

Figure 13. The tensile ductility is plotted as a function of the grain boundary diffusion compensated strain rate for several fine-grained UHC steels.

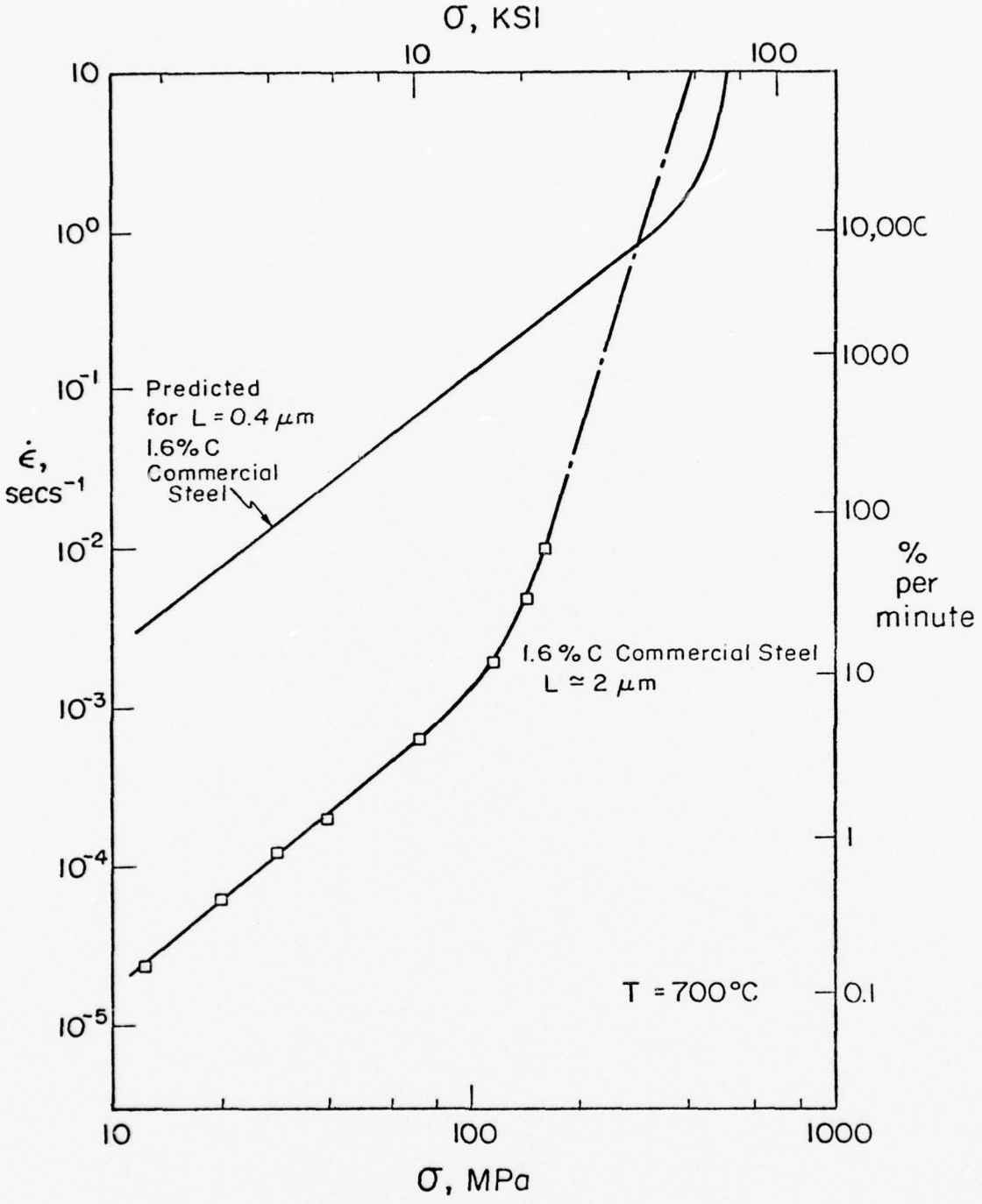

Figure 14. The predicted flow stress-strain rate relation is shown for a 1.6%C steel for a stable grain size of 0.4μm at 700°C. Under these conditions superplastic flow should be observed at strain rates as high as one per second.

The Pressure Sintering Kinetics of Iron Powders and Superplastic Ultrahigh Carbon Steel Powders

Robert D. Caligiuri

THE PRESSURE SINTERING KINETICS OF IRON POWDERS AND SUPERPLASTIC ULTRAHIGH CARBON STEEL POWDERS

by

Robert D. Caligiuri

The purpose of this investigation was to study the pressure sintering kinetics of metal powders. Specifically, this investigation has focused on the kinetics of pressure sintering of iron powders and ultrahigh carbon steel powders that contain a superplastic microstructure. The important results and conclusions of this study are outlined in the following paragraphs.

An ultrafine grain structure, in the order of one micron in size, is generally accepted as a necessary prerequisite for superplastic behavior. Previous research at Stanford has shown that ultrafine grain size stabilized by discrete second phase particles of cementite can be produced in ultrahigh carbon steels. The techniques developed to produce such microstructures can be classified into two groups: mechanical (involving hot and warm working of the material) and thermal (involving quenching and annealing of the material). These techniques are discussed in detail elsewhere [1-5]. Utilizing this work, the present investigation centers on two methods of generating superplastic microstructures in ultrahigh carbon steel powders, one mechanical and the other thermal. The mechanical method involves building the desired superplastic microstructure into bulk material by hot and warm working, followed by milling and attriting into powder form. This method was very successful in producing superplastic 1.6%C steel powders, but proved to be time consuming and inefficient. As a result, the thermal method was developed. It was shown that vacuum-annealing 1.22%C and 1.76%C steel liquid atomized (water quenched) powders at 700°C for one hour converted the fully martensitic microstructures (Figure 1 and 2) into fine, spheroidized microstructures (Figure 3 and 4). The thermal method proved to be a simple, rapid technique for producing large

quantities of superplastic powders.

The influence of microstructure on densification behavior was illustrated by compacting 1.6%C steel fine structure powders (produced by the mechanical method as shown in Figure 5) at 650°C and 69 MPa -- a temperature and pressure where this fine structure steel is known to behave superplastically (see Figure 6). The resulting density* - time plot was compared to the density-time plot of powders similarly pressed but produced from the as-cast (coarse structure) 1.6%C steel. The microstructure of the coarse structure powders is shown in Figure 7. The two density-time curves are shown in Figure 8. After 4 hours, the 1.6%C steel fine structure compact is about 95% dense while the 1.6%C steel coarse structure compact is only about 87% dense. A similar difference in densification response between the fine structure (superplastic) and coarse structure (non-superplastic) powders is observed at other warm temperatures and low pressures. From these results it is concluded that a superplastic microstructure enhances densification and permits the pressing of high density compacts at warm temperatures and low pressures.

The kinetics of the densification process during warm pressing were studied in order to determine why superplastic microstructures enhance densification. Detailed measurements of the relative density-time behavior of liquid atomized commercially pure iron powders and liquid atomized vacuum-annealed ultrahigh carbon steel powders were made. These measurements premitted determination of densification rate as a function of density, temperature, and applied pressure. These data, shown in Figures 9, 10 and 11, lead to the following phenomenological equation for densification rate ($\dot{\rho}$) during the intermediate stage of densification (between 80 and 95% relative density):

---

* All references to density in this report are relative densities; that is, the actual density in gm/cm^3 divided by the theoretical density in gm/cm^3.

$$\dot{\rho} = \frac{K}{b^2} \left(\frac{1-\rho}{\rho}\right)^t D \left(\frac{P_A}{E}\right)^t \qquad (1)$$

where K is a material constant, b is the Burgers vector, ρ is the relative density, D is the self-diffusion coefficient (lattice self-diffusion for the iron powders and grain boundary self-diffusion for the ultrahigh carbon steel powders), t is a material dependent exponent, E is Young's modulus, and P_A is the applied pressure. A literature search reveals that other workers [6-10] have observed the dependence of densification rate on the self-diffusion coefficient and the power law dependence on applied pressure. However, this investigation appears to have been the first to suggest and to demonstrate that the densification rate during the intermediate stage of densification depends on relative density according to the parameter $\left(\frac{1-\rho}{\rho}\right)^t$. This parameter was chosen initially because it predicts that the densification rate should go to zero as $\rho \to 1$ and should be equal to infinity as $\rho \to 0$ -- both physically realistic limits. Analyses showed that, in addition to the data of this investigation, this parameter also describes the available data on alumina powders [11], copper -1% alumina powders [12], and cobalt oxide powders [9].

The presence of the self-diffusion coefficient in the phenomenological densification rate equation indicates that densification by warm pressing (during the intermediate stage, at least) is diffusion controlled. To be more specific as to the actual microscopic deformation mechanism involved (i.e. dislocation motion, grain boundary sliding, stress assisted diffusion, etc.), it is necessary to determine the steady state creep properties of the materials studied. Compression creep studies on samples machined from high density compacts were thus performed and showed that the commercially pure iron and ultrahigh carbon steels obey the usual power law relationship between the steady state creep rate ($\dot{\varepsilon}_{ss}$) and the flow stress (σ):

$$\dot{\varepsilon}_{ss} = \frac{A}{b^2} D \left(\frac{\sigma}{E}\right)^n \qquad (2)$$

where A is a material constant, b is the Burgers vector, D is the self-diffusion coefficient (lattice self-diffusion coefficient for the commercially pure iron and grain boundary self-diffusion for the ultrahigh carbon steels), n is the stress exponent, and E is Young's modulus. Below $\frac{\sigma}{E} \simeq 5 \times 10^{-4}$, the stress exponent for the iron is about 4 and is about 2.5 for the ultrahigh carbon steels. Comparison of the material constants in Equation (1) to the material constants in Equation (2) revealed that $t \simeq n$ and $K \simeq 56.7A$ (56.7 is the average of the values of the three materials studied). Taking $\sigma = P_A$ as a basis for comparison, the intermediate stage densification rate can then be related to the steady state creep rate at a given temperature:

$$\dot{\rho} = 56.7 \left(\frac{1-\rho}{\rho}\right)^n \dot{\varepsilon}_{ss} \qquad (3)$$

Thus, for a fixed value of relative density the intermediate stage densification rate at a given warm temperature and low pressure is directly proportional to the steady state creep rate of the material at the same warm temperature and low pressure. Equation (3) holds for cobalt oxide and alumina as well (Figure 12). It is therefore concluded that the mechanism which controls steady state creep at the given stress, temperature and microstructure also controls the intermediate stage of densification under similar conditions. Other workers [12-19] have stressed the importance of steady state creep mechanisms during densification, specifically the intermediate stage, but this work appears to have been the first to establish a quantitative relationship between creep rate and densification rate. With this relationship the densification behavior of a material can be predicted by simply knowing its creep properties at the temperature and pressure of interest.

The relationship between densification rate and creep rate (Equation (3)) was next studied in more detail to understand better the enhancement of densification found with superplastic microstructures. Since superplastic materials generally creep faster than non-superplastic materials at warm temperatures and

low stresses, Equation (3) predicts that superplastic materials will densify faster than non-superplastic materials during warm pressing. This in fact was observed with the 1.6%C powders (Figures 6 and 8). The relationship between densification rate and creep rate further predicts through the term $(\frac{1-\rho}{\rho})^n$ that, at the same creep rate, superplastic materials (low stress exponent) will densify faster than non-superplastic materials (high stress exponent). This prediction was verified experimentally. First, creep experiments were performed to determine the stress at 650°C where superplastic 1.6%C steel has the same steady state creep rate as the non-superplastic commercially pure iron. This stress is 43.1 MPa as shown in Figure 13. Powders of these materials were then compacted at 43.1 MPa and 650°C for 4 hours. After correction for the initial stage of densification, the 1.6%C superplastic powders are about 3 percent more dense than the iron powders, as seen in Figure 14. Thus the term $(\frac{1-\rho}{\rho})^n$ does contribute significantly to the enhancement of densification by superplastic microstructures.

An attempt was made to give the term $(\frac{1-\rho}{\rho})^n$ some physical meaning. Based on Equation (1), a new expression for the average effective stress for densification (σ_E) was introduced:

$$\sigma_E = (\frac{1-\rho}{\rho})\ P_A \qquad (4)$$

where P_A is the applied pressure. We believe this expression accounts for the effect of both porosity and die wall constraining forces on the average stress actually causing material to flow into the pores. Using Equation (4) and taking $\sigma = \sigma_E$ as a basis for comparing creep behavior to densification behavior, the relationship between densification rate and creep rate can now be reduced to:

$$\dot{\rho} = 56.7\ \dot{\varepsilon}_{ss} \qquad (5)$$

From this equation it is concluded that, for a constant effective stress (hence constant $\dot{\varepsilon}_{ss}$), the intermediate stage densification rate will not vary with

relative density. In other words, the dependence on relative density of densification rate observed in this and other investigations is due solely to the decrease in effective stress. Other researchers [11,17,20,21,22] have advanced expressions for the effective stress in terms of the applied pressure, but this investigation apparently has been the first to advance an expression based on experimental data which predicts that the effective stress is less than the applied pressure and decreases to zero as the porosity goes to zero ($\rho \rightarrow 1$). The results of this investigation suggest a new approach towards the future theoretical development of an expression for effective stress, using Equation (4) as a guide.

Further examination of Equation (5) reveals that, at a constant effective stress where a superplastic and non-superplastic material have the same steady state creep rate, there should be no difference in densification behavior during the intermediate stage. This is verified by using Equations (4) and (5) to compute the ratio, at a given value of relative density, between the densification rate of the 1.6%C steel superplastic powders and the densification rate of the commercially pure iron powders warm pressed at 650°C and 43.1 MPa. This computed ratio can then be compared to the experimentally measured ratio at that density (Figure 14). The computed ratios match the measured ratios very well. It is therefore concluded that the enhancement of densification during warm pressing observed with a superplastic microstructure can be completely accounted for by the faster creep rates at low stresses (resulting from a different deformation mechanism) characteristic of superplastic materials. The extremely high ductility associated with superplastic materials apparently does not influence the densification process. The above results are also indirect evidence that Equation (4) is the correct expression for effective stress. More direct evidence can be provided by performing pressure sintering experiments under constant effective stress conditions, and then determining whether or not the relative

density-time curves for the superplastic and non-superplastic materials superimpose over the intermediate stage.

Three different theoretical models for the densification behavior during the intermediate stage of densification were next investigated. These models proved to be variations on the same theme -- control of intermediate stage densification by the mechanisms of power law creep. Of the three models studied, the model of Wilkinson and Ashby [16] fits the experimental data the best. This model also predicts that materials with a stress exponent of 2.5 should densify faster than materials with a stress exponent of 4. The Wilkinson-Ashby equation, however, does not fit the experimental data very well (Figures 15,16 and 17). The problem with the model can be traced to the prediction of the relative density dependence of the densification rate and is attributable to the unrealistic assumption of a hydrostatic stress uniformly collapsing the pores. A more realistic description, however, is likely possible only with a finite element approach to determing the stress and strain rate fields around an arbitrarily shaped collapsing pore. Developement of such a finite element code would be a very interesting research problem and worthy of future study.

This research has shown that powders containing a superplastic microstructure can be pressed to very high densities at warm temperatures and low pressures. This concept has potential commercial applications. As a result, several areas of applications were examined. One such application is a method of producing bulk superplastic materials by warm pressing superplastic powders without a protective atmosphere. Determination of the feasibility of this method requires that the residual porosity and oxides present in warm pressed iron and ultrahigh carbon steels on room temperature mechanical properties be studied. It was thus demonstrated that the small amount of oxide absorbed into the matrix along former particle boundaries does not reduce the compressive ductility of these materials

(Figure 18). The 2.5% residual porosity in the ultrahigh carbon steels does, however, cause a decrease in yield strength. It is therefore concluded that warm pressing superplastic powders in air is a feasible P/M forming technique.

The feasibility of forming cast irons by P/M techniques was next considered. As shown in Figure 19, the liquid atomized 2.6% white cast iron powders after heating to 700°C contain pockets of superplastic-like ferrite and cementite surrounded by a network of proeutectoid cementite. Change in strain rate tests and stress relaxation tests performed at 650°C on a sample machined from a virtually 100% dense white cast iron compact yielded a stress exponent of about 3.3. This low stress exponent indicates a tendency towards superplastic deformation. This white cast iron compact also exhibited normal room temperature properties, a yield strength of 700 MPa (102,000 psi) and a 5% compressive strain before fracture [23,24]. The resulting density and mechanical properties are better than those obtained by earlier workers [25,26] on cast irons. This difference can be attributed to two factors. First, the times used by the early workers (less than one minute) were too short for high densification by creep (intermediate stage densification) to occur. Second, the early workers used hot pressing temperatures above the eutectoid transformation temperature. Any fine structure developed during processing was thus lost. Hence, their cast iron powders were much stronger than the 2.6%C white cast iron powders used in this investigation. The general conclusion is that, under appropriate conditions of time, pressure and temperature, P/M warm pressing is a feasible way of shaping brittle cast iron.

The solid state weldability of mild steels and ultrahigh carbon steels was also studied. It was shown that two 1.6%C steel plates, after proper cleaning and polishing, can be successfully welded by pressing them together in air at 650°C under 69 MPa of pressure for 3 hours (Figure 20). Mild steel

plates, similarly cleaned and pressed, do not successfully weld (Figure 21). The high ease of solid state weldability of the ultrahigh carbon steel plates is attributable to two factors. One is that the grain boundaries present provide many sources of high atom mobility paths for iron atom bonding. The second factor is that the weak ultrahigh carbon steel can flow into the asperities (pores) readily. Although the ultrahigh carbon steel plates are solidly joined, a line seems to demarcate the interface (Figure 20). Examination at higher magnifications shows this line to consist of flattened grain boundaries and carbide particles which tend to grow across the interface as time progresses (Figure 22). The good solid state weldability of ultrahigh carbon steels also extends to multi-layer stacks as well as two-layer stacks. This research has shown for the first time that steel plates can be successfully welded in air below 700°C and may open up a whole new area of warm temperature solid state welding technology.

REFERENCES

1. O. D. Sherby, B. Walser, C. M. Young, and E. M. Cady, "Superplastic Ultrahigh carbon Steel," Scripta Met., 9, 569 (1975).

2. E. S. Kayali, "Superplasticity of Eutectoid Steel and Iron-Carbon Alloys," Ph.D. Dissertation, Department of Mat. Sci. and Engr., Stanford University, Stanford, Ca. (May 1976).

3. O. D. Sherby, C. M. Young, B. Walser, E. M. Cady, "Superplastic Ultrahigh Carbon Steel," U.S. Patent #3,951,697, April 20, 1976.

4. B. Walser, E. S. Kayali, and O. D. Sherby, "Warm Working and Superplasticity in Plain Ultrahigh Carbon Steels," 4th International Conference on the Strength of Metals and Alloys," Nancy, France, Vol. I, ed. by Laboratoire de Physique de Solide - E.N.S.M.I.M. (August 1976).

5. B. Walser and O. D. Sherby, "Superplastic Ultrahigh Carbon Steels," Second Annual Report submitted to Advanced Research Projects Agency, Washington, D.C. (August 1975).

6. J. Williams, "The Hot Compacting of Metal Powders," in Symposium on Powder Metallurgy, 1954, ed. by Iron and Steel Institute, London (1956).

7. T. Vasilos and R. M. Spriggs, "Pressure Sintering: Mechanisms and Microstructures for Alumina and Magnesia," J. Amer. Ceram. Soc., 46, 493 (1963).

8. F. E. Westermann and R. G. Carlson, "Hot Pressing of Lead Spheres," Trans. Met. Soc. AIME, 221, 649 (1961).

9. P. A. Urick and M. R. Notis, "Final-Stage Densification During Pressure-Sintering of CoO," J. Amer. Ceram. Soc., 56, 570 (1973).

10. J. G. Early, F. V. Lenel, and G. S. Ansell, "The Material Transport Mechanism During Sintering of Copper-Powder Compacts at High Temperatures," Trans. Met. Soc. of AIME, 230, 1641 (1964).

11. R. C. Rossi and R. M. Fulrath, "Final Stage Densification in Vacuum Hot Pressing of Alumina," J. of Amer, Ceram. Soc., 48, 558 (1965).

12. W. Beeré, "The Role of Sequential Processes in the Hot Pressing of Copper/Alumina," Acta Met., 24, 277 (1976).

13. M. S. Koval'chenko and G. V. Samsonov, Poroshkovaya Metallurgica, 1, No. 2, 3 (1961).

14. S. Scholz and B. Lersmacher, Asch. Eisenhuttenwesen, 41, 98 (1964).

15. R. L. Coble and J. S. Ellis, "Hot-Pressing Alumina--Mechanisms of Material Transport," J. Amer. Ceram. Soc., 46, 438 (1963).

16. D. S. Wilkinson and M. F. Ashby, "Pressure Sintering by Power Law Creep," Acta Met., 23, 1277 (1975).

17. R. L. Coble, "Diffusion Models for Hot Pressing With Surfact Energy and Pressure Effects as Driving Forces," J. App. Physics, 41, 4798 (1970).

18. F. V. Lenel and G. S. Ansell, "Creep Mechanisms and Their Role in the Sintering of Metal Powders," in Modern Developments in Powder Metallurgy, Volume I: Proceedings of the 1965 International Powder Metallurgy Conf., ed. by H. H. Hausner (1965).

19. W. Beeré, "Diffusional Flow and Hot Pressing: a Study of MgO, " J. Mat. Sci., 10, 1434 (1975).

20. J. D. McClelland, "Kinetics of Hot Pressing," Powder Metallurgy: Proc. of Inter. Conf. in New York, ed. by W. Leszynski, 157, Interscience Purlishers, New York (1961).

21. R. M. Spriggs and T. Vasilos, "Functional Relation Between Creep Rate and Porosity for Polycrystalline Ceramics," J. Amer. Ceram. Soc., 47, 47, (1964).

22. P. L. Farnsworth and R. L. Coble, "Deformation Behavior of Dense Polycrystalline SiC," J. Amer. Ceram. Soc., 49, 264 (1966).

23. R. D. Caligiuri, R. T. Whalen, and O. D. Sherby, "Superplastic Hot Pressing of White Cast Iron," International Journal of Powder Metallurgy, 12, 9, (1976).

24. American Society for Metals, Metals Handbook, Eighth Edition, Volume I: "Properties of Selection of Metals," 401 (1961).

25. W. D. Jones, Foundry Trade Journal, 39, 401 (1938).

26. F. Sauerwald and S. Kubik, "Uber Synthetische Metallkorper," Z. Elektrochem., 38, 33 (1932).

(A)

(B)

Screen Analysis for Liquid Atomized 1.22%C Steel Powders

	Tyler Screen Mesh Size, μ						
	<45	45	64	75	106	150	180
Percent of charge weight trapped	27.4	15.2	13.4	13.2	7.6	10.5	12.7

(C)

Figure 1. Characterization of the liquid atomized 1.22%C steel powders. (A) shows the unetched powders as received. The powders are "spheroid" in shape. (B) shows the microstructure of one of the as recieved particles after etching. Note that it is martensitic. (C) shows the results of the Tyler Screen Analysis. The average particle size is about 70μm.

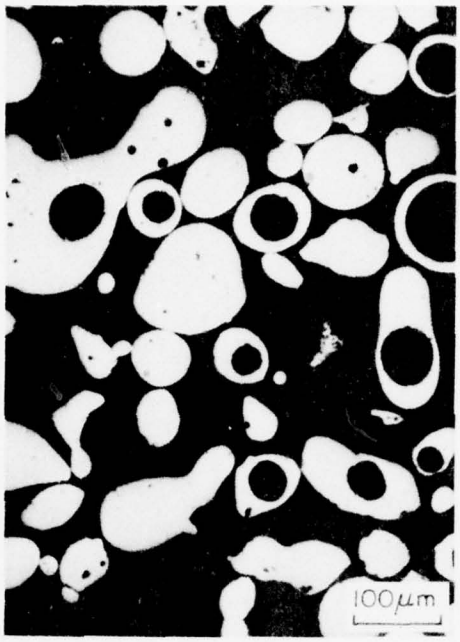

(A)

(B)

Screen Analysis for Liquid Atomized 1.76%C Steel Powders

	Tyler Screen Mesh Size, μ						
	<45	45	64	75	106	150	180
Percent of charge weight trapped	22.1	14.4	13.7	14.2	8.8	12.3	14.6

(C)

Figure 2. Characterization of the liquid atomized 1.76%C steel powders. (A) shows the unetched powders as received. The powders are "spheroid" in shape. (B) shows the microstructure of one of the as-received particles after etching. Note that it is martensitic. (C) shows the results of the Tyler Screen Analysis. The average particle size is about 70μm.

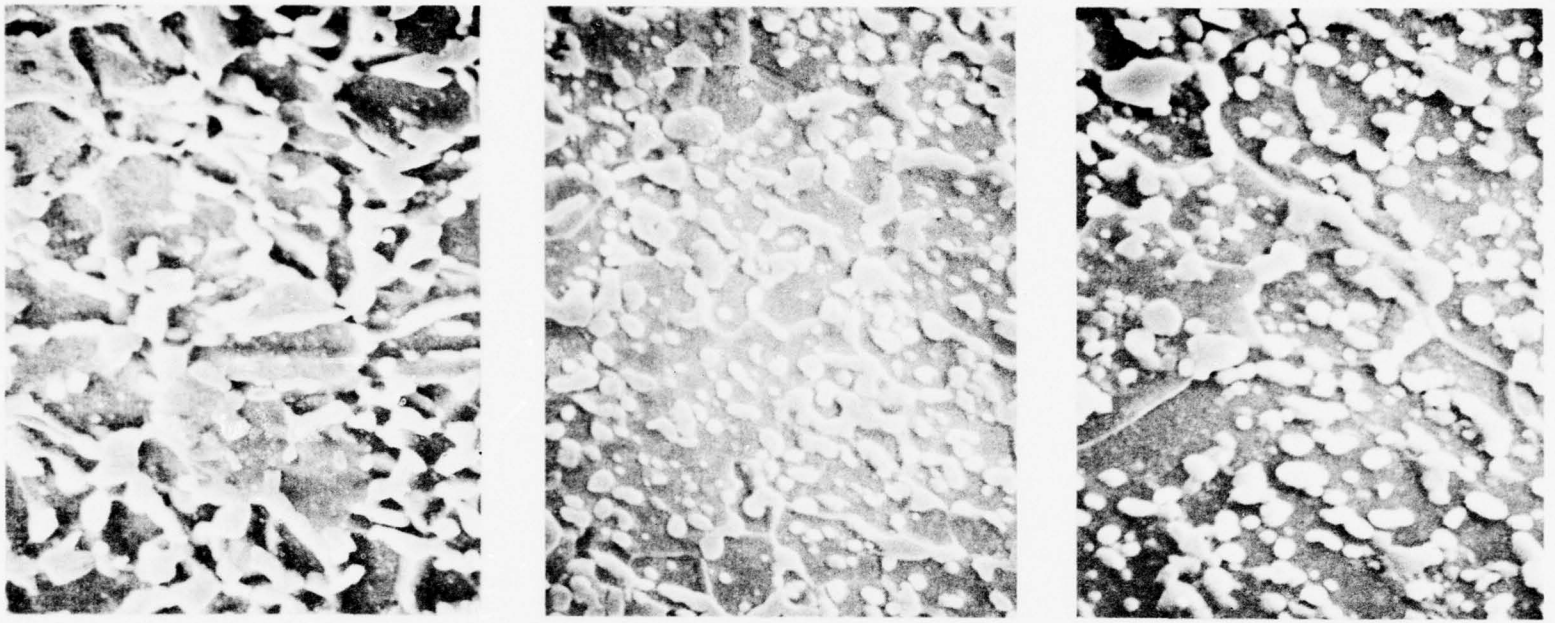

Figure 3. Vacuum annealing studies on liquid atomized 1.22%C steel powders. Temperature of anneal was 700°C. (A) shows the microstructure of one particle after annealing for 0.5 hours, (B) the microstructure after 1 hour and (C) the microstructure after 1.5 hours. One hour was determined to be the optimum annealing time.

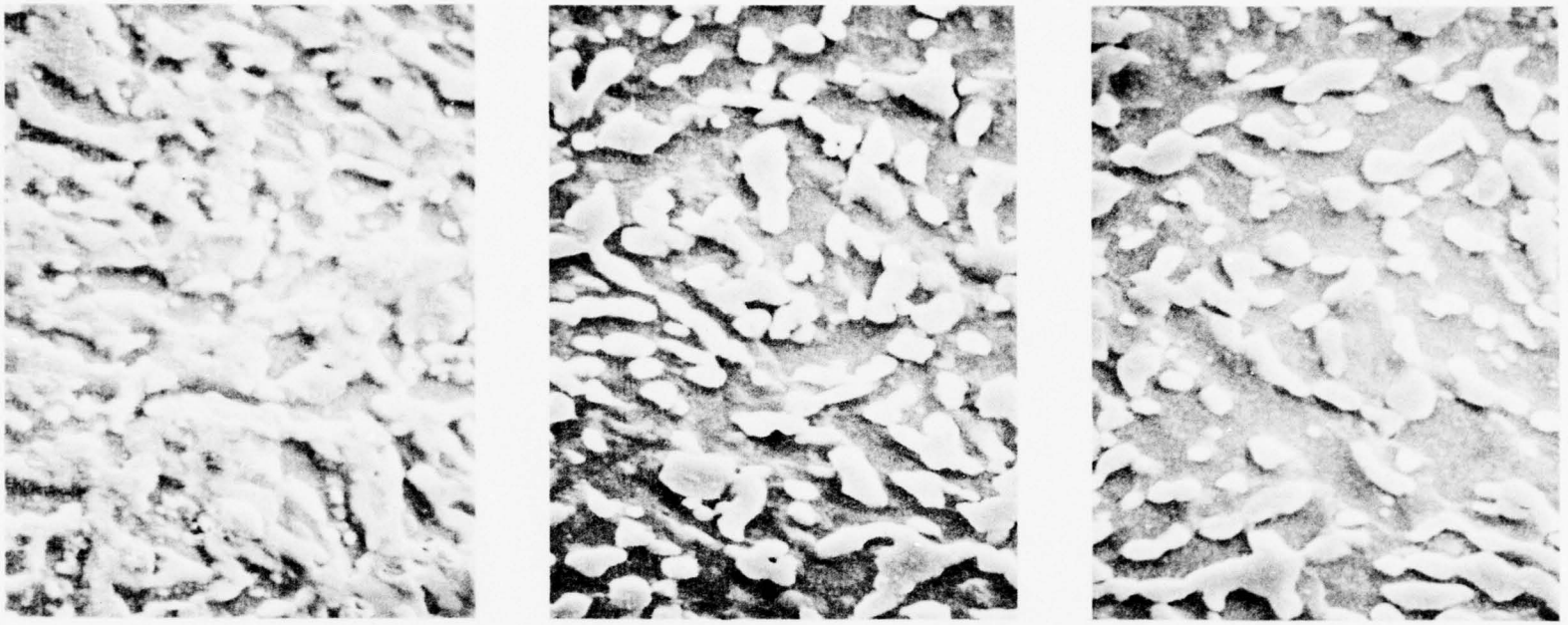

Figure 4. Vacuum annealing studies on liquid atomized 1.76%C steel powders. Temperature of anneal was 700°C. (A) shows the microstructure of one particle after annealing for 0.5 hours, (B) the microstructure after 1 hour, and (C) the microstructure after 1.5 hours. One hour was determined to be the optimum annealing time.

(A)

(B)

Screen Analysis for 1.6%C Steel Atrrited Fine Structure Powder

	Tyler Screen Mesh Size, μ						
	<45	45	64	75	106	150	180
Percent of charge weight trapped	17.1	10.5	6.8	20.5	25.1	15.9	4.1

(C)

Figure 5. Characterization of the 1.6%C steel attrited fine structure powders. (A) shows the unetched powders after attrition. The particles are "angular" in shape. (B) shows the microstructure of one particle detailing the fine structure (less than two micron grain size) present. (C) Shows the Tyler Screen Analysis results. The average particle size is around 100μm.

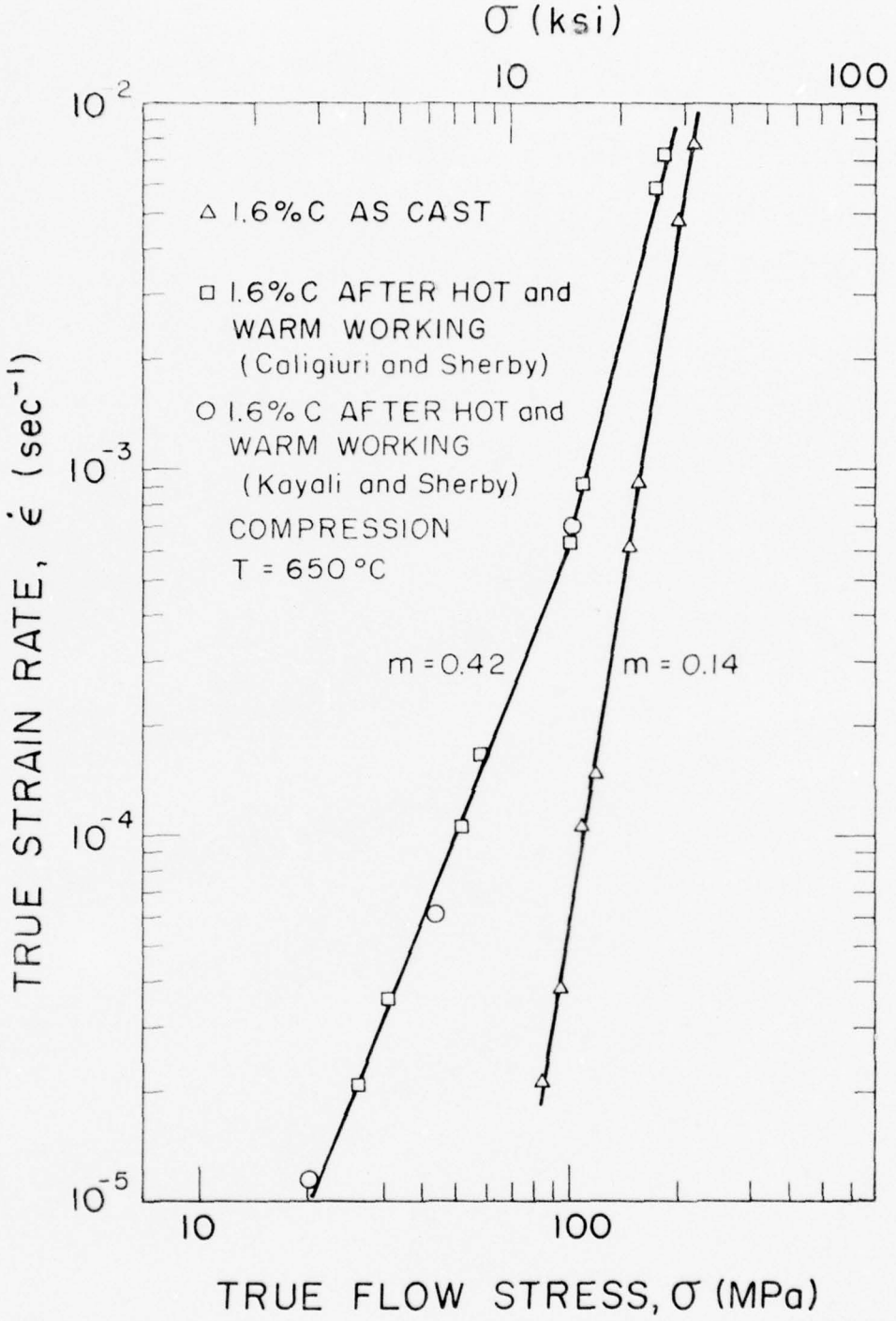

Figure 6. True flow stress-true strain rate relationship for the 1.6%C steel both in the as cast condition (Figure 3.7(A)) and after hot and warm working (Figure 3.7(B)). The strain rate sensitivity exponent for the worked material below a stress of 10 MPa is about 0.42. Also shown is the data of Kayali [6] on hot and warm worked 1.6%C superplastic steel. It matches very well the data collected in this investigation.

(A)

(B)

Screen Analysis for 1.6%C Steel Attrited Coarse Structure Powder

	Tyler Screen Mesh Size, μ						
	<45	45	64	75	106	150	180
Percent of charge weight trapped	19.8	8.9	5.9	21.1	26.4	15.0	2.9

(C)

Figure 7. Characterization of the 1.6%C steel attrited coarse structure powders. (A) shows the unetched powders after attrition. They are "angular" in shape. (B) shows the microstructure of one particle detailing the coarse carbide structure present. (C) shows the results of the Tyler Screen Analysis. The average particle size is about 100μm.

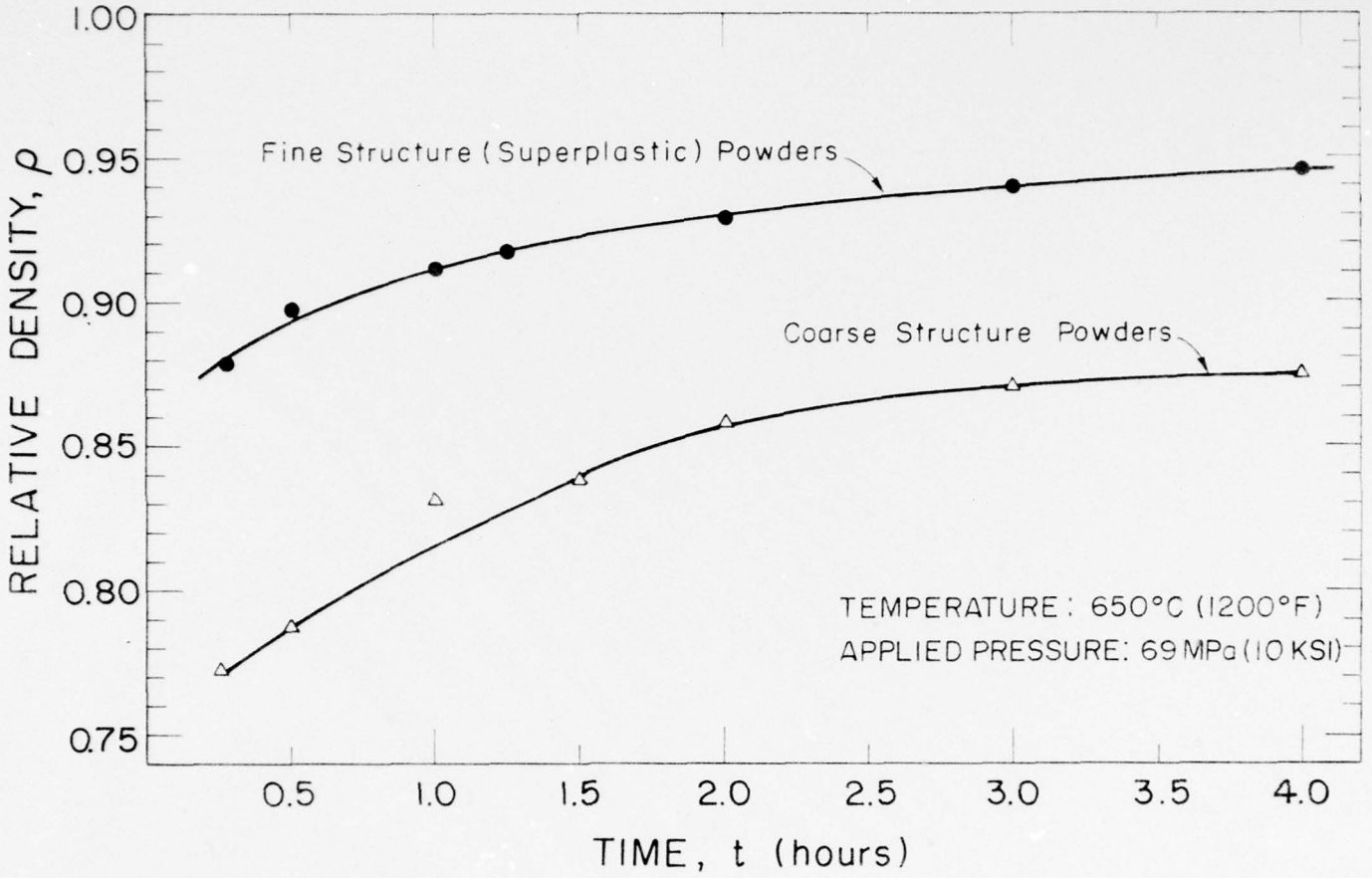

Figure 8. Relative density-time plots for the 1.6%C steel attrited fine structure powders and coarse structure powders; each was compacted at 650°C and 69 MPa. The fine structure powders are consistently 7 to 8% more dense than the coarse structure powders throughout compaction. Initial relative density for both compacts was 60%.

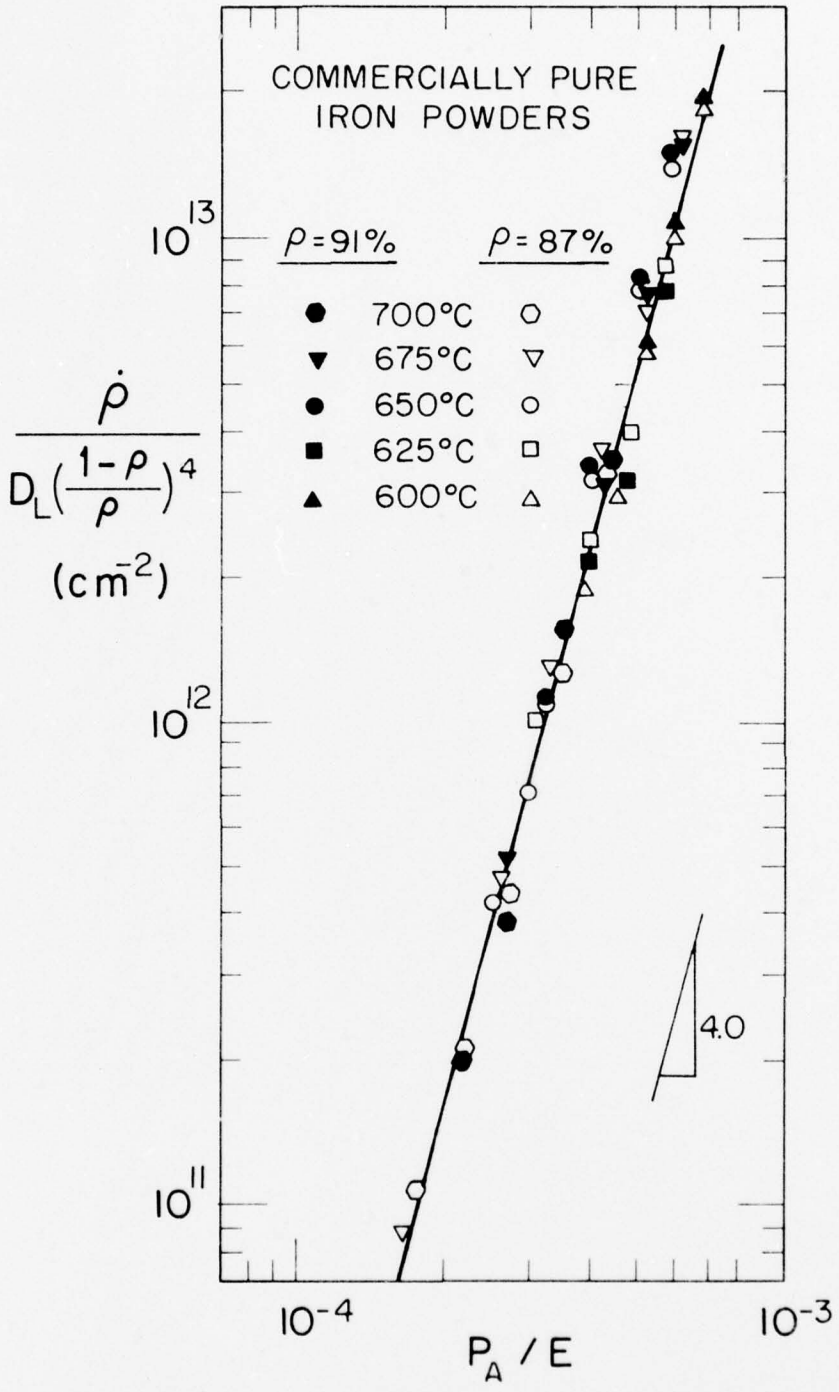

Figure 9. Demonstration of the validity of the phenomenological relation (Equation (26)) in accurately describing the densification rate behavior of the commercially pure iron powders during the intermediate stage of densification. D_L is the lattice self-diffusion coefficient.

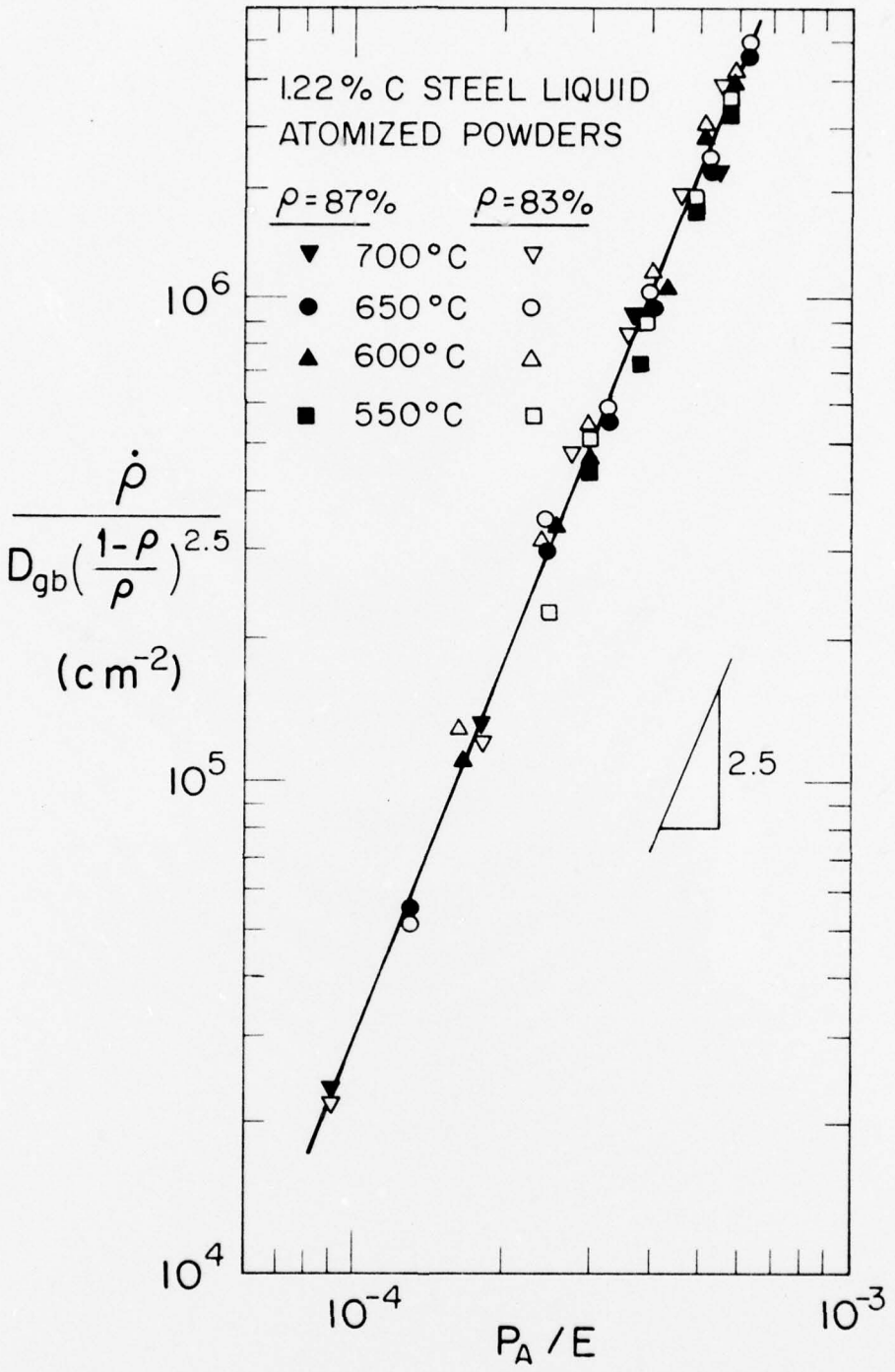

Figure 10. Demonstration of the validity of the phenomenological relation (Equation (31)) in accurately describing the densification rate behavior of the 1.22%C steel liquid atomized powders during the intermediate stage of densification. D_{gb} is the grain boundary self-diffusion coefficient.

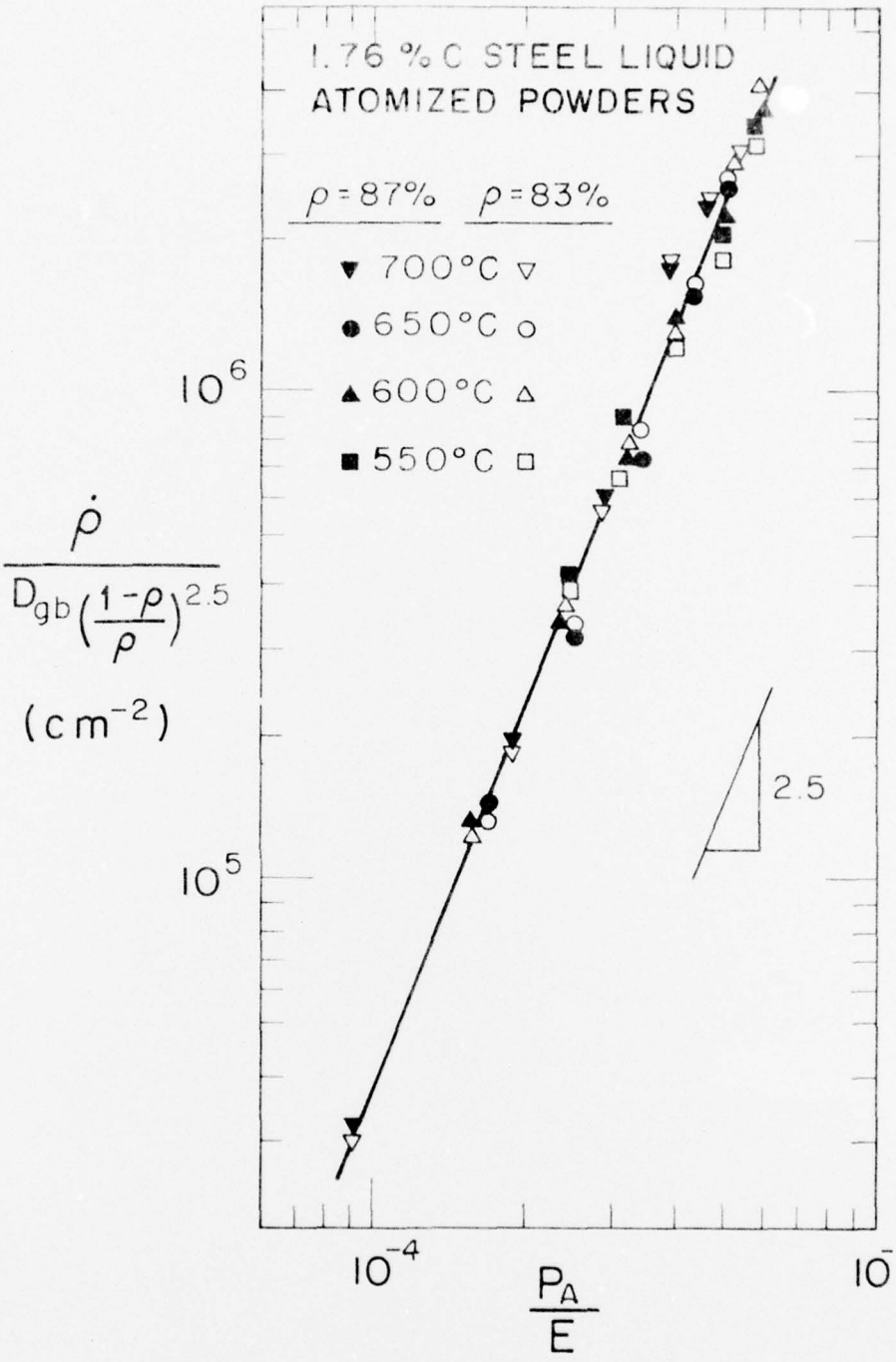

Figure 11. Demonstration of the validity of the phenomenological relation (Equation (31)) in accurately describing the densification rate behavior of the 1.76%C steel liquid atomized powders during the intermediate stage of densification. D_{gb} is the grain boundary self-diffusion coefficient.

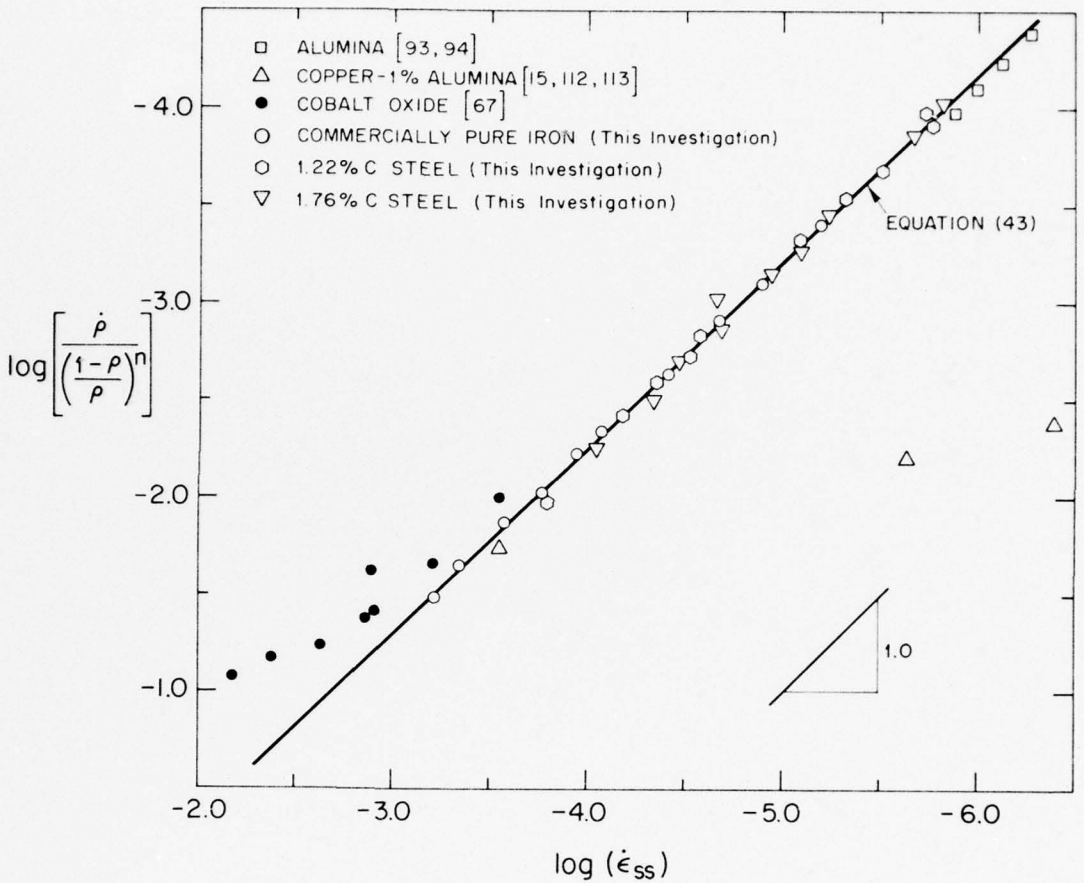

Figure 12. The relationship between densification rate and steady state creep rate for all presently available data. The solid line is the prediction of Equation (43): it has a slope of one and an intercept of log (56.7) = 1.75. The failure of the copper/ 1% alumina to fit the prediction can be attributed to the uncertainty in the steady state creep data.

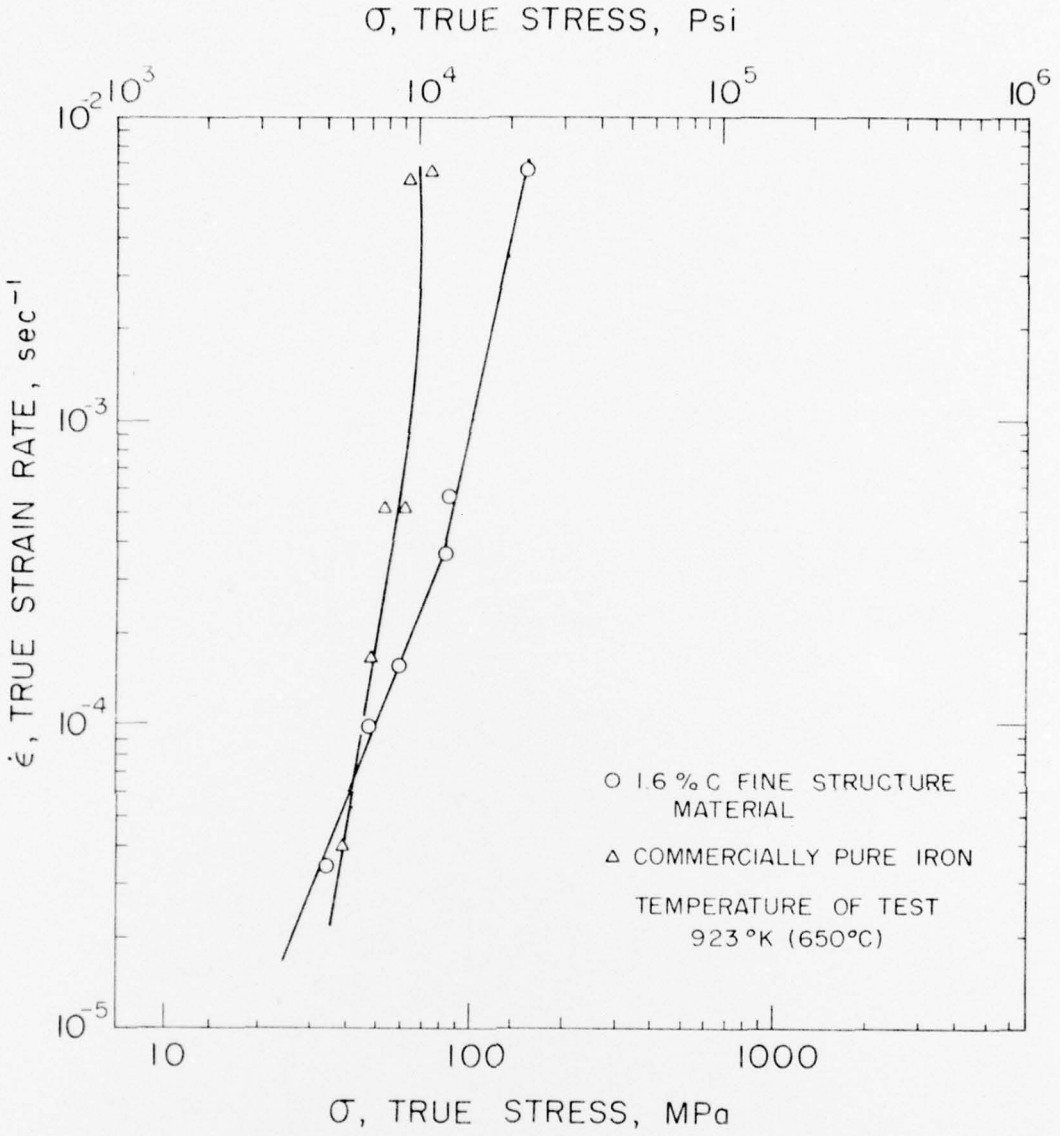

Figure 13. Plots of the steady state creep rate ($\dot{\varepsilon}_{ss}$) - flow stress (σ) behavior for both the 1.6%C fine structure material and the commercially pure iron material at 650°C. This shows that both materials have the same steady state creep rate at a flow stress of 43.1 MPa.

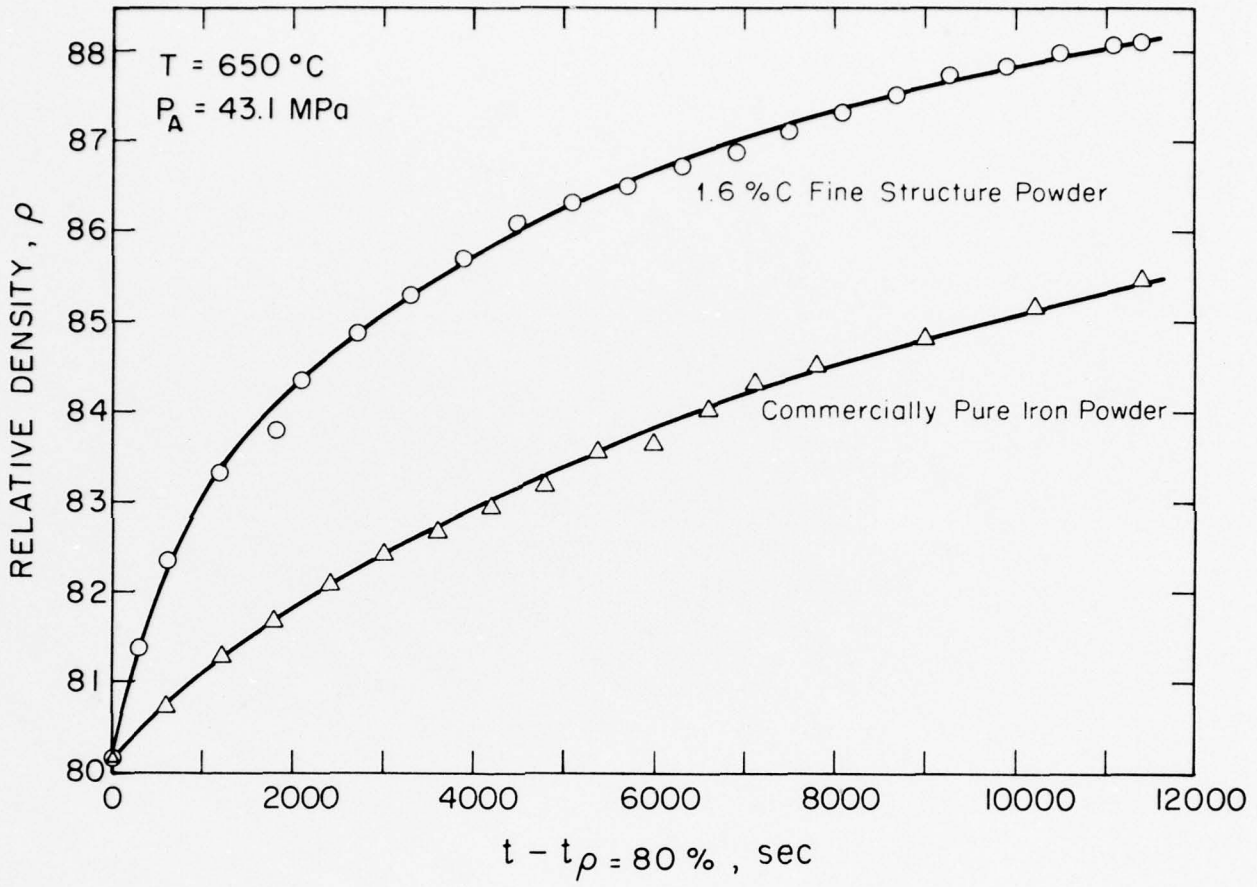

Figure 14. Relative density-time behavior of the 1.6%C fine structure (superplastic) powders and the commercially pure iron powders compacted at 650°C and at a constant applied pressure of 43.1 MPa. The data has been corrected so as to exclude the initial stage of densification.

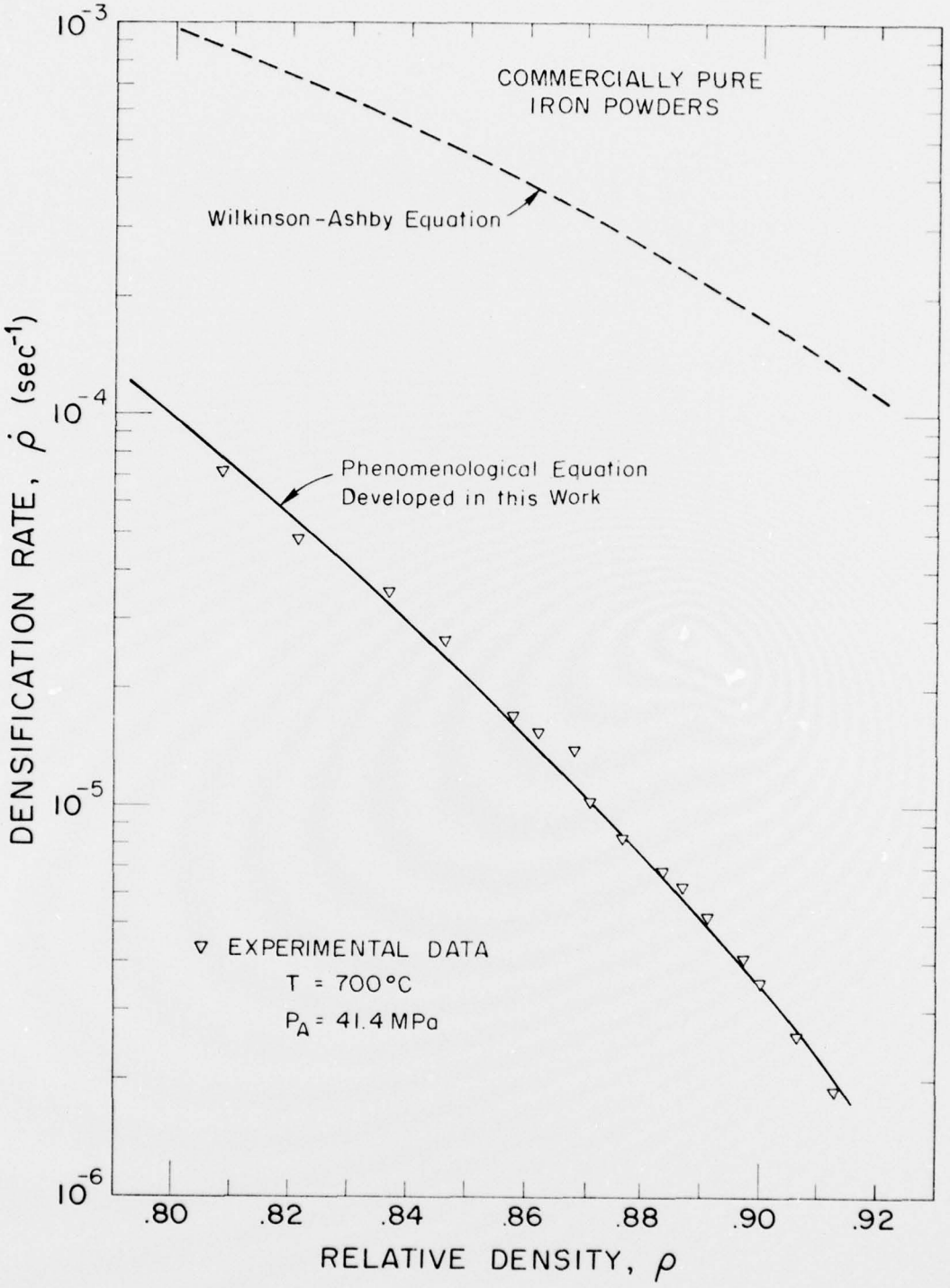

Figure 15. Comparison of experimental data with the Wilkinson-Ashby prediction of the dependence of densification rate ($\dot{\rho}$) on relative density (ρ) for the commercially pure iron powders.

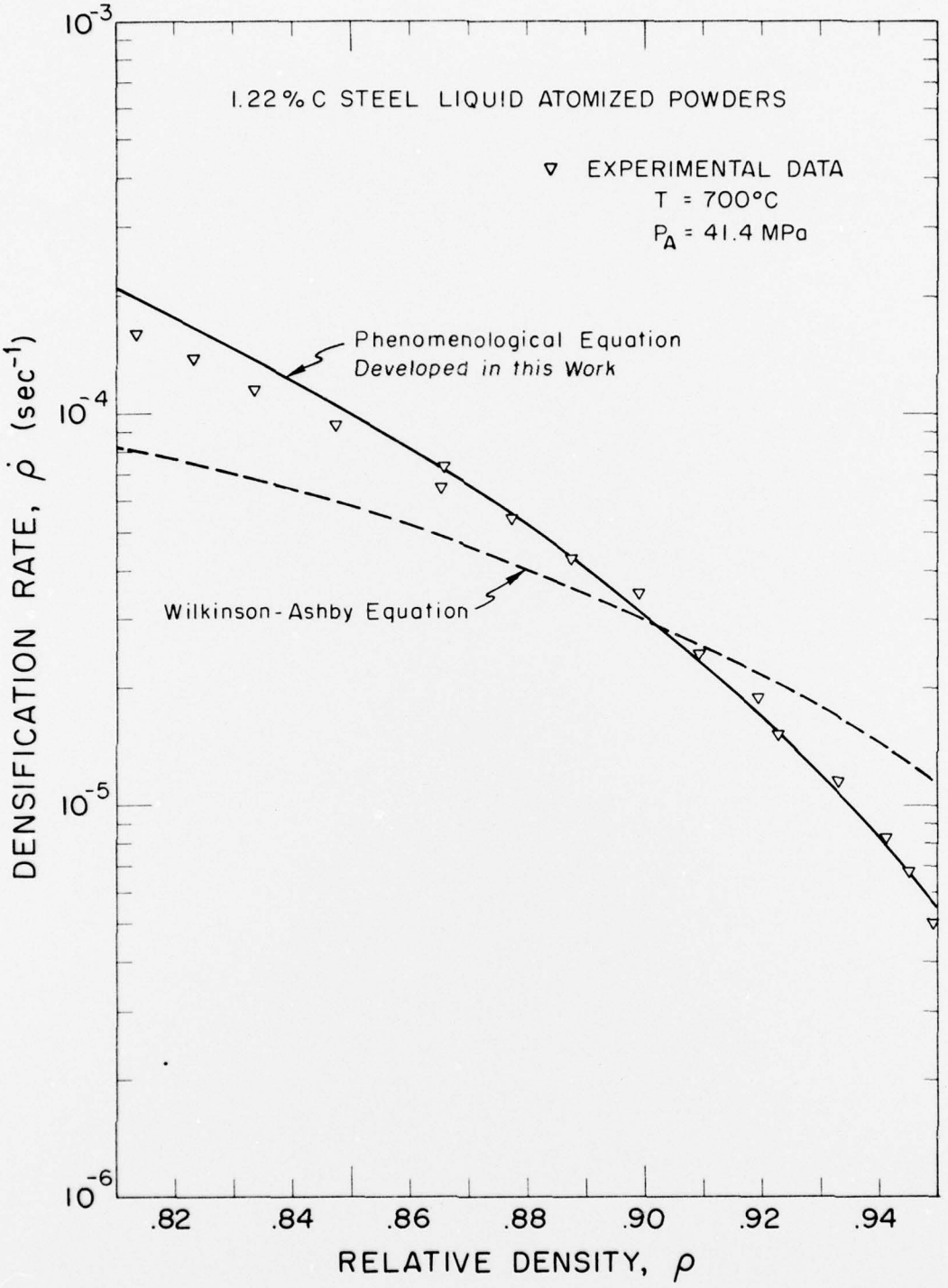

Figure 16. Comparison of experimental data with the Wilkinson-Ashby prediction of the dependence of densification rate ($\dot{\rho}$) on relative density (ρ) for the 1.22%C steel liquid atomized powders.

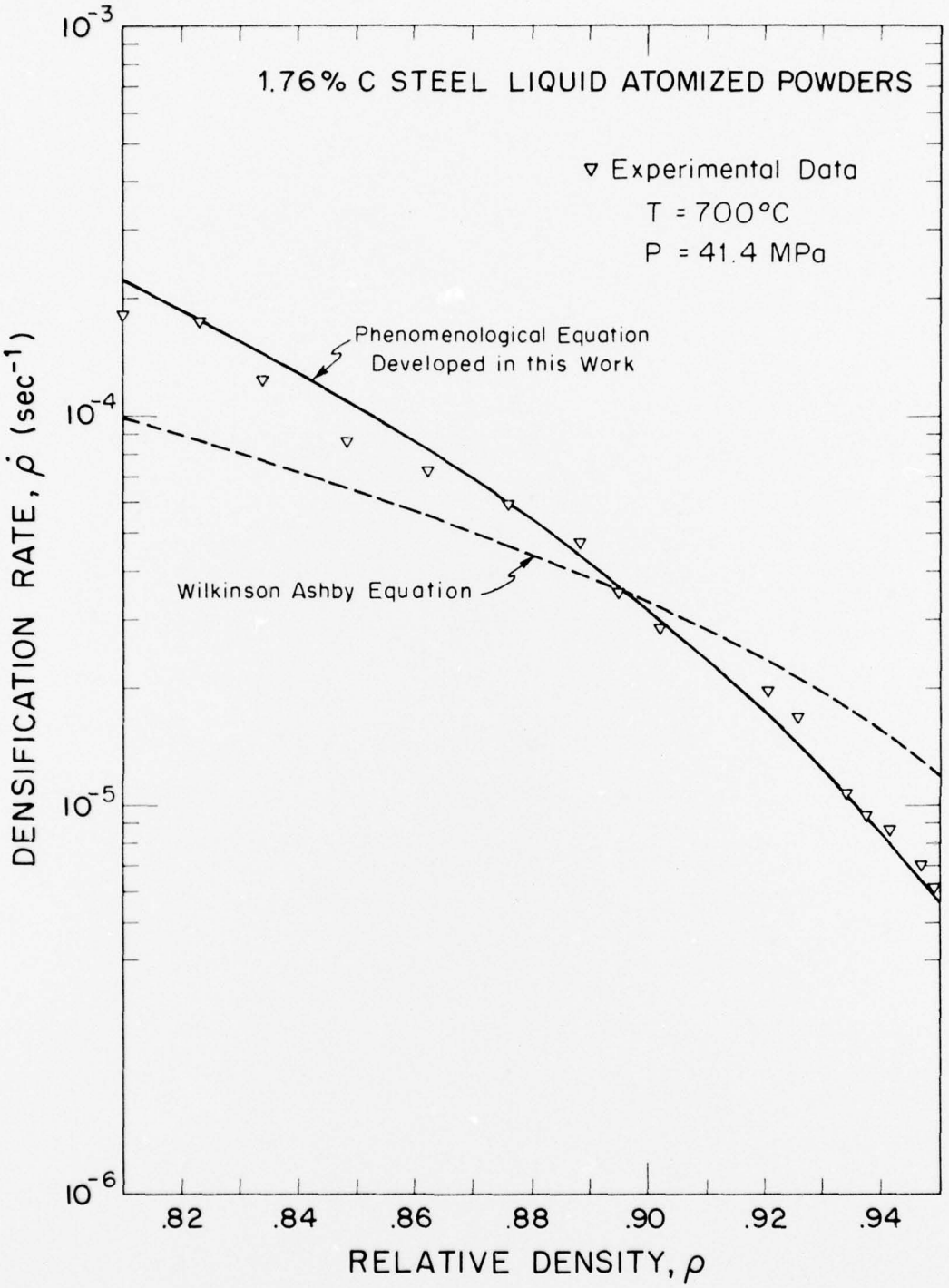

Figure 17. Comparison of experimental data with the Wilkinson-Ashby prediction of the dependence of densification rate ($\dot{\rho}$) on relative density (ρ) for the 1.76%C steel liquid atomized powders.

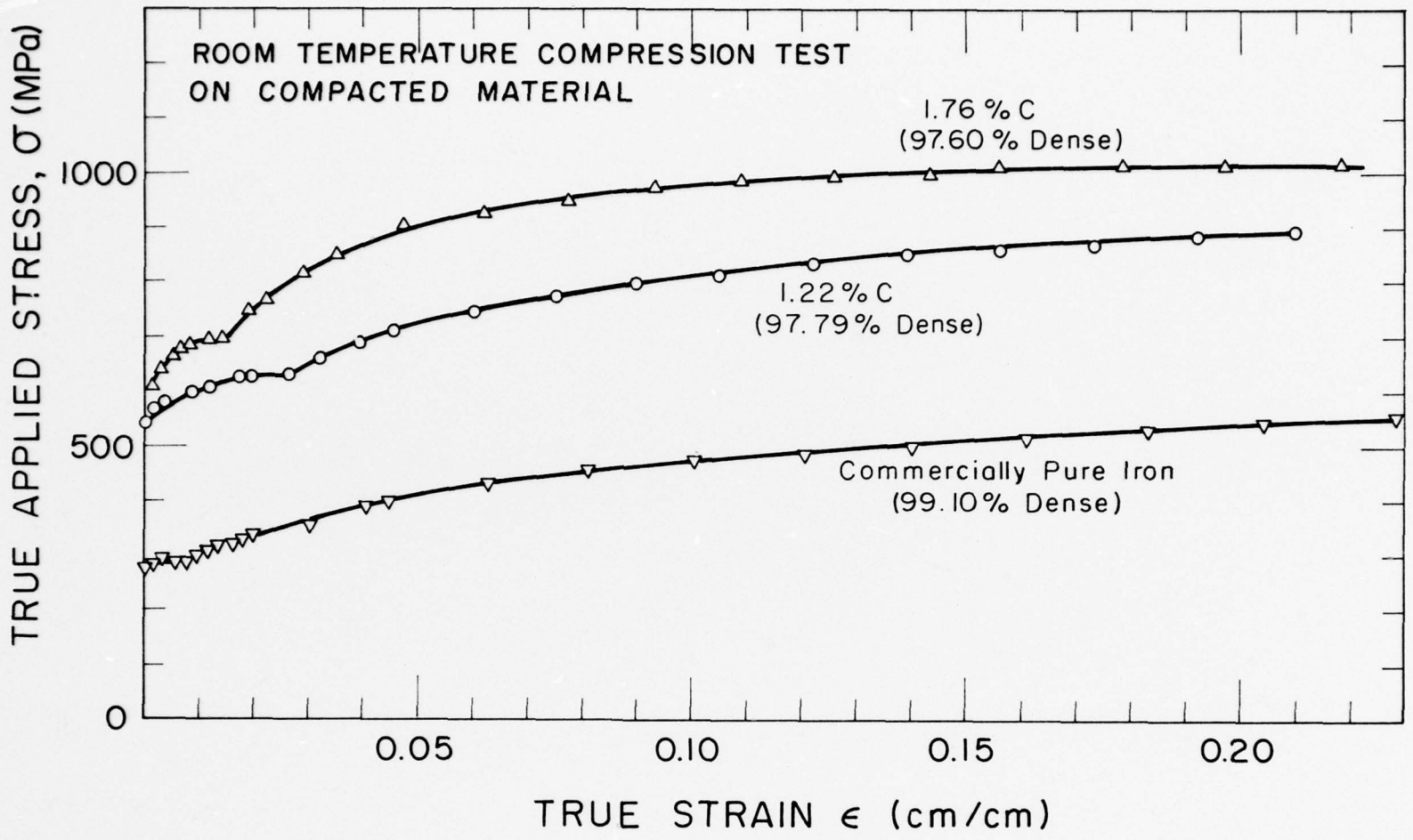

Figure 18. Room temperature compression true stress-true strain behavior for three compacted materials studied in this investigation. For each sample, the relative density after compaction(but prior to testing)is given.

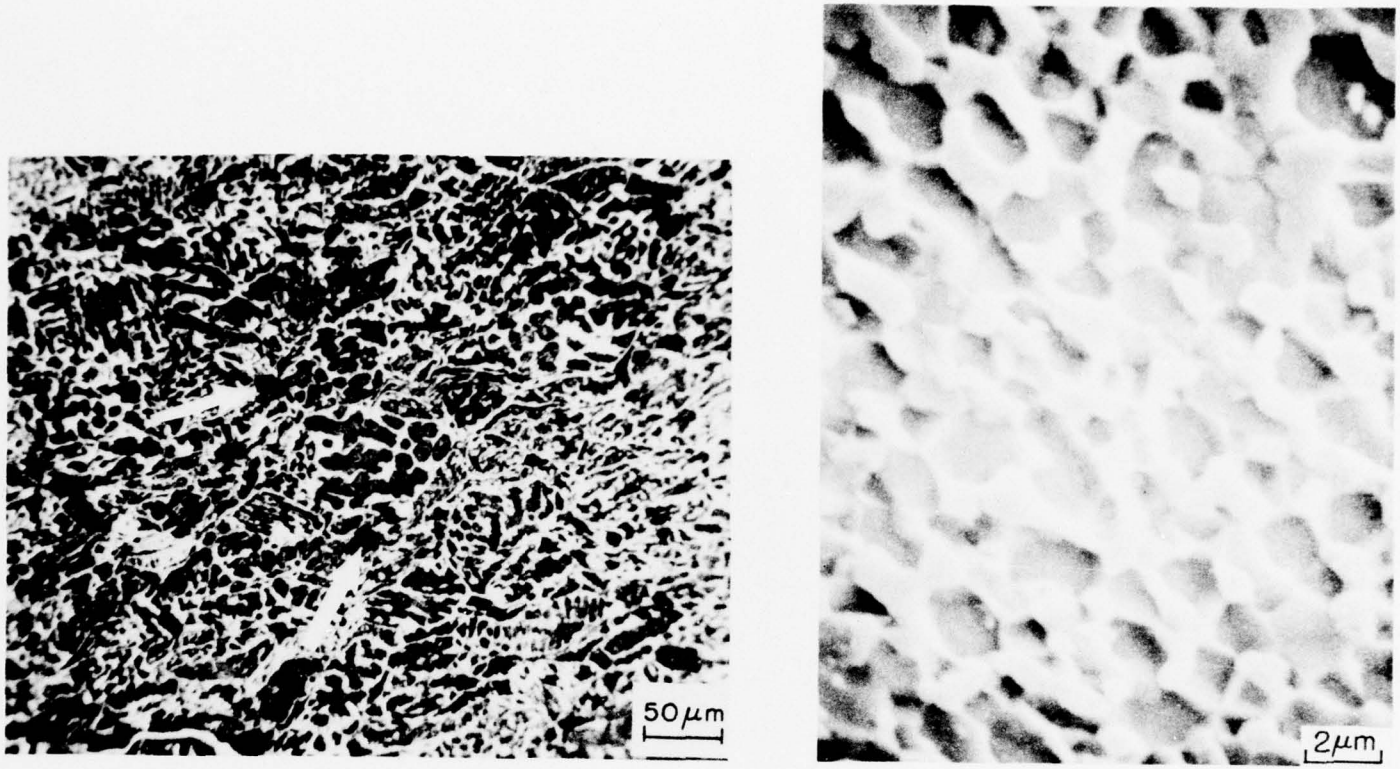

Figure 19. Microstructure of a 2.6% white cast iron compact after warm pressing at 700°C and 69 MPa for 5 hours to a final relative density of 95%. (A) shows the former ledeburite colonies dispersed in a matrix of proeutectoid cememtite. The arrows point out two such colonies. (B) details the structure of one of these colonies. The structure consists of fine ferrite grains (<2μm) stabilized by fine spheroidized cementite particles (<1μm).

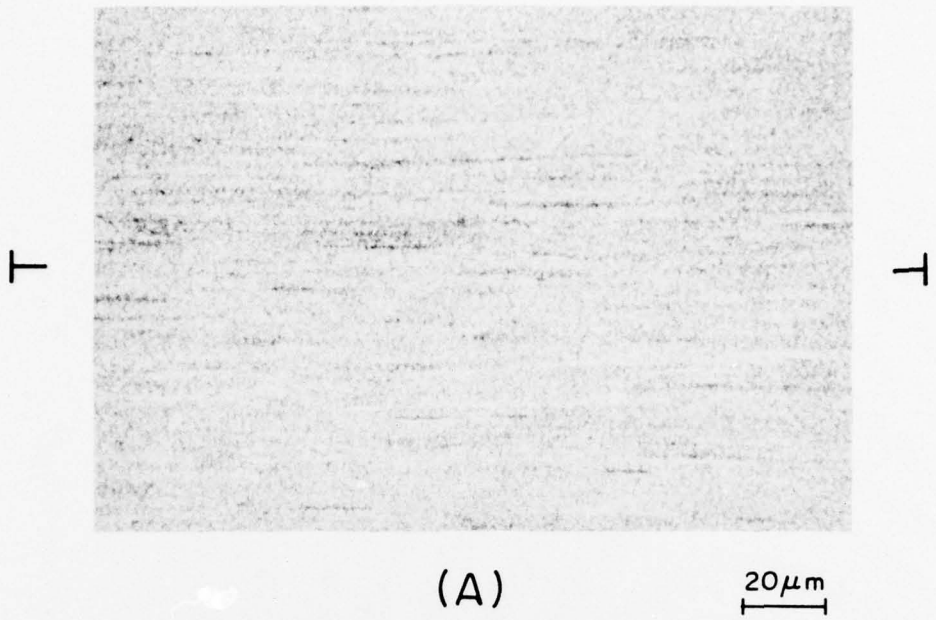

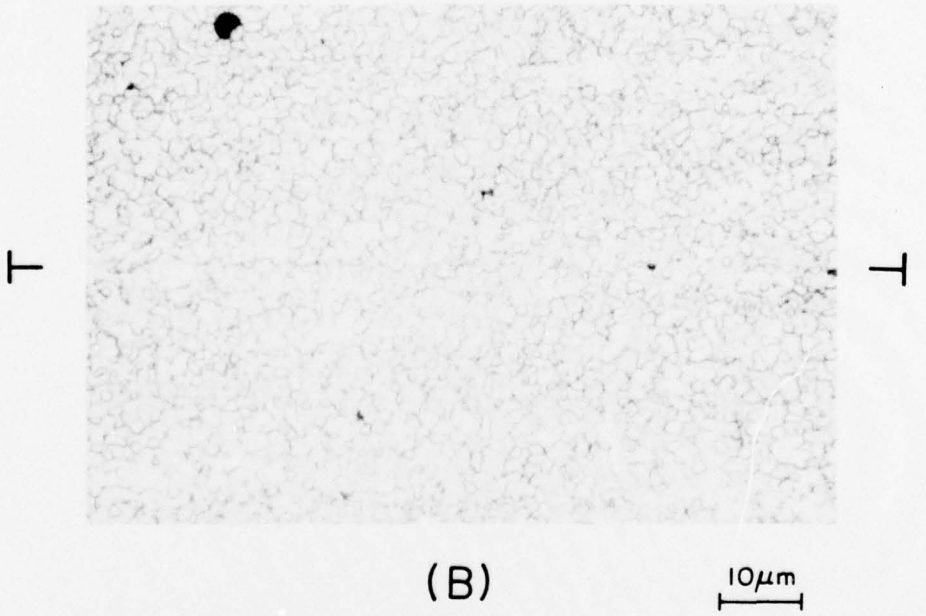

Figure 20. The interface between two 1.6%C steel plates solid state welded in air at 650°C and 69 MPa for three hours. (A) shows the plates to be well joined -- no evidence of residual asperities or oxides. The interface is indicated by tic marks at the sides of the micrograph. (B) shows no residual asperities or oxides at high magnification. Some sort of line does seem to mark the interface, however. The large black spots in the matrix are graphite particles.

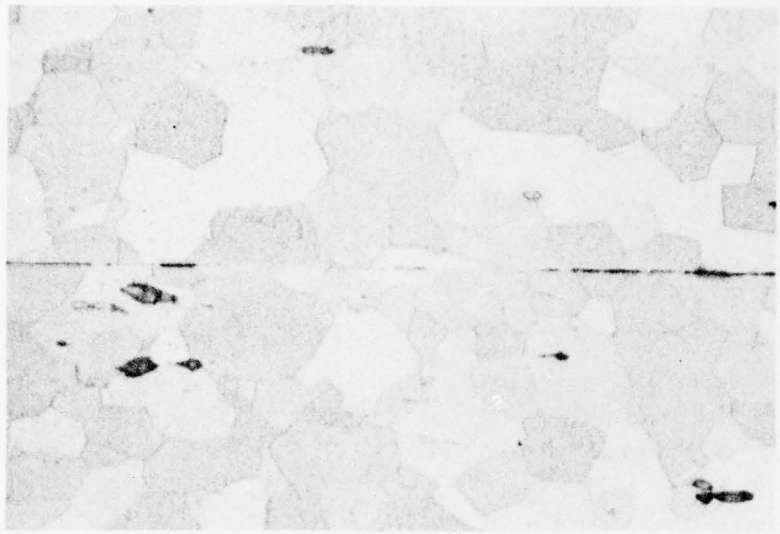

(A) 200μm

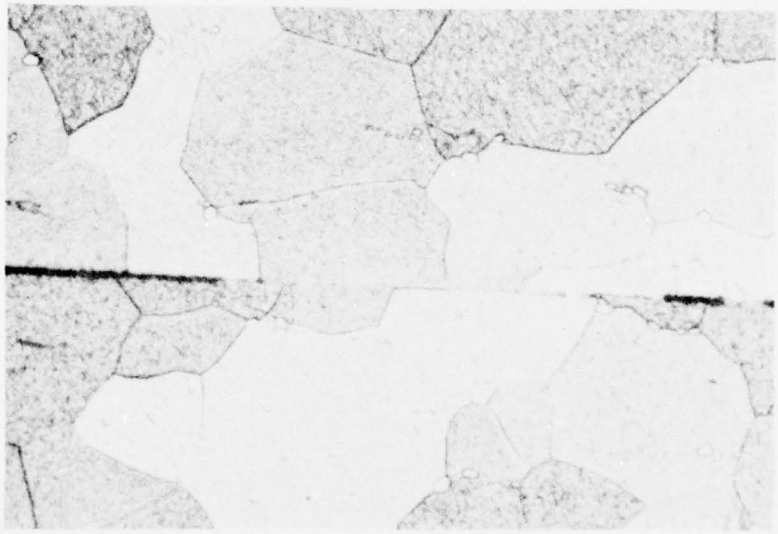

(B) 10μm

Figure 21. The interface between two AISI 1005 mild steel plates solid state welded in air at 650°C and 69 MPa for three hours. In (A) the plates are seen to be poorly joined and show many residual asperities. (B) shows the interface at higher magnification. The residual asperities likely contain oxides.

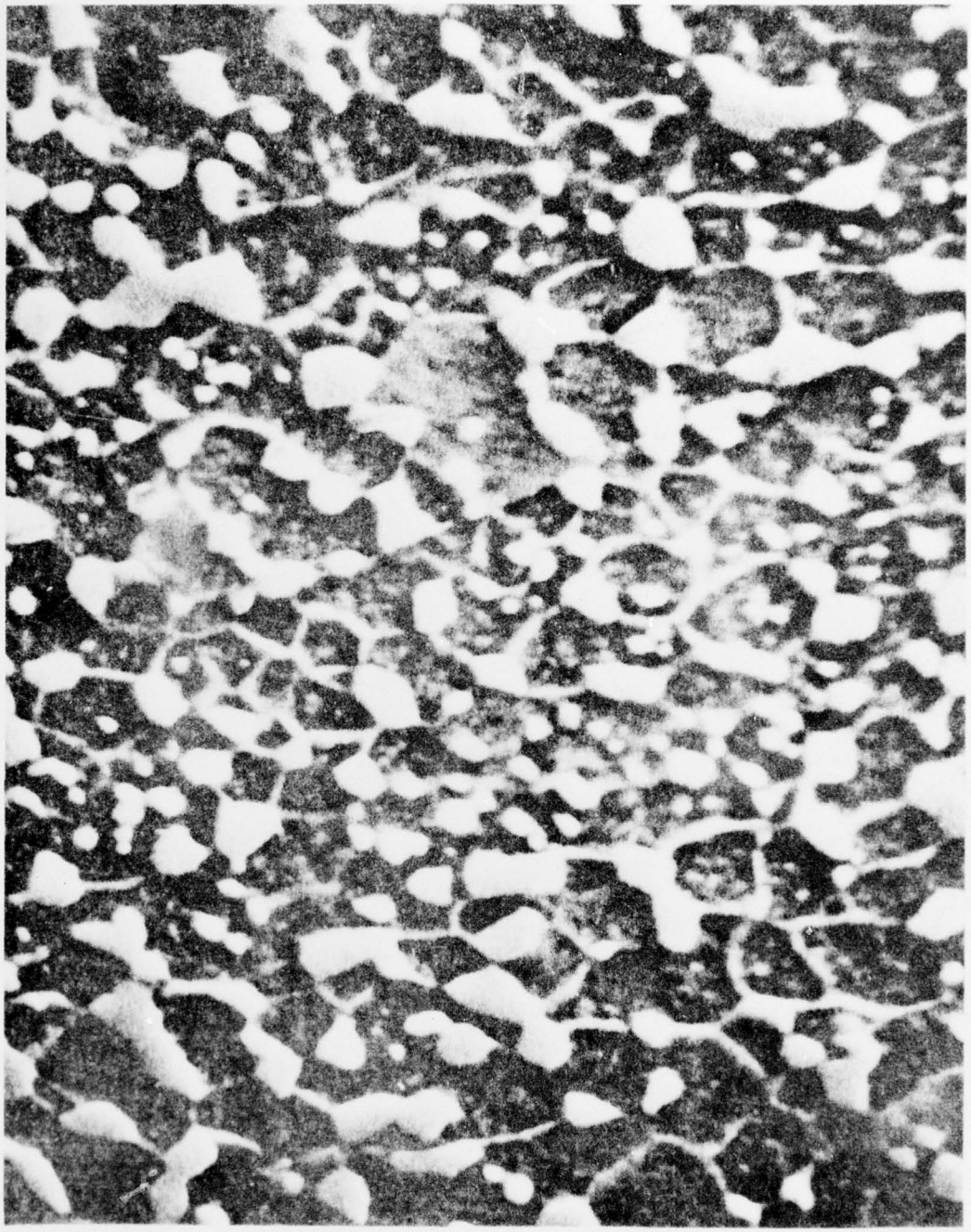

Figure 22. A SEM micrograph of the interface region shows the line visible in Figure 6.4(B) to consist of flattened carbide particles and grain boundaries. The line disappears in places because of grain growth. All trace of the interface would disappear if held at temperature for a sufficient length of time.